Properties of Atoms in Molecules: Atoms Forming Molecules

Jesús Hernández-Trujillo[†] and Richard F. W. Bader*

Department of Chemistry, McMaster University, Hamilton, Ontario L8S 4M1, Canada

Received: November 17, 1999; In Final Form: January 5, 2000

This paper studies the evolution of the electron densities of two separated atoms into an equilibrium molecular distribution. A range of interactions is considered: from closed-shell with and without charge transfer, through polar-shared, to equally shared interactions. The changes in the density are monitored in terms of the properties of the density at the bond critical point and the shape of the interatomic surface. The effect of these changes on the properties of the atoms defined as proper open systems is determined. The "harpoon mechanism" operative in the formation of LiF is found to exert dramatic effects on the electron density and on the atomic and molecular properties. The virial and the Ehrenfest force theorems in their molecular, atomic, and local forms, together with the Hellmann−Feynman theorem, provide an understanding of the similarities and differences in the bonding resulting from closed-shell, shared, and polar interactions. The effect of the long-range dispersion forces on the electron density and the resulting changes in the kinetic and potential energies, the former decreasing and the latter increasing on the initial approach of the atoms, are investigated. In addition to the changes in the total energy and its kinetic and potential energy components as a function of the internuclear separation R, the atomic contributions to these quantities are also reported. The atomic Ehrenfest force is the force acting on the electron density in an atomic basin and the one measured in an atomic force microscope. It is shown to change from an intially attractive interaction, to a repulsive one at a separation slightly greater than R_e where the Hellmann−Feynman forces on the nuclei vanish.

Mechanism Of Chemical Bonding

This paper studies the changes in the electron density $\rho(\mathbf{r})$ and the accompanying changes in the atoms and their properties in the formation of diatomic molecules. The cases studied cover a wide range of atomic interactions: from the limit of a shared interaction found in the formation of H_2 and N_2, to the closed-shell ionic limit in the formation of LiF, together with the intermediate polar interaction encountered in the formation of CO. The interaction of two closed-shell atoms without charge transfer to yield a van der Waals molecule is illustrated by the formation of Ar_2. The changes in the properties of the molecule encountered during bonding are equated to those of the participating atoms using the physics of a proper open system to define the atoms.[1,2] A proper open system is a region of real space bounded by a surface $S(\mathbf{r}_s)$ of local zero-flux in the gradient vector field of the electron density, as denoted in eq 1

$$\nabla\rho(\mathbf{r})\cdot\mathbf{n}(\mathbf{r}) = 0 \quad \forall\ \mathbf{r} \in S(\mathbf{r}_s) \tag{1}$$

Equation 1 serves as the boundary condition for the definition of an open system using the principle of stationary action. The atoms of chemistry are identified with proper open systems because: (1) their properties are characteristic and additive, summing to yield the corresponding values for the molecule, and (2) they are as transferable from one system to another as are the forms of the atoms in real space, that is, as transferable as are their charge distributions. In particular, the atomic and group properties defined in this manner predict the experimentally determined contributions to the volume, energy, polarizability, and magnetic susceptibility in those cases where the group contributions are essentially transferable, as well as additive.[3]

The approach of two atoms results in the formation of a critical point (CP) in the density, a point where $\nabla\rho(\mathbf{r}) = \mathbf{0}$ and where the density attains its minimum value along the axis of approach. It is a CP of rank 3 and signature −1, a (3, −1) CP. The interatomic surface $S(\mathbf{r}_s)$ is defined by the set of trajectories of $\nabla\rho(\mathbf{r})$ constructed from the eigenvectors associated with the two negative eigenvalues of the Hessian of ρ that terminate at the CP, while the unique pair of trajectories defiined by the positive eigenvalue and which originate at the CP define a line of maximum density linking the nuclei of the two atoms. For a molecule in a bound state the CP is termed the bond CP and the line of maximum density the bond path. Nuclei linked by a bond path are also linked by a virial path, a line of maximally negative potential energy density, and, for a diatomic molecule, the two paths are coincident. Nuclei linked by a bond path are bonded to one another.[4] The position of the bond CP relative to the nuclear positions and the shape of the interatomic surface are determined by the flux in the electronic momentum density and transfer of charge through the surface resulting from the interaction between the two atomic basins. Thus the formation of the bond CP and of the interatomic surface is a direct consequence of the interaction between the two atoms, and their changing properties isolate the essential features of the interaction. Properties of the density at a bond CP are subscripted with a "b", such as ρ_b and $\nabla^2\rho_b$.

Atomic Theorems. The physics of an open system Ω, which includes as a particular case the total system bounded at infinity, is governed by the equation of motion for each of the observables, which for a stationary state reduces to eq 2 for the observable $\hat{G}(\mathbf{r})$,[1,2]

[†] Permanent address: Departamento de Física y Química Teórica, Facultad de Química, Universidad Nacional Autónoma de México, México D. F. 04510, México.

10.1021/jp994096z CCC: $19.00
Published on Web 02/05/2000

$$^1/_2\{(i/\hbar)\langle\psi[\hat{H},\hat{G}(\mathbf{r})]\psi\rangle_\Omega + cc\} = {}^1/_2\oint dS(\Omega,\mathbf{r})\mathbf{j}_G(\mathbf{r})\cdot\mathbf{n}(\mathbf{r}) + cc \quad (2)$$

where $\mathbf{j}_G(\mathbf{r})$ is the current density for property G. Unlike the total system with its boundary at infinity, the average of the commutator $[\hat{H},\hat{G}]$ does not vanish for an open system, but is instead equal to the flux in the current density of $\hat{G}(\mathbf{r})$ through its bounding surface. This balance of basin and surface contributions is a necessary consequence of a system being in a stationary state, since the time rate of change of the property G over the open system is determined by their difference.

It is important to note that while $\hat{H}$ is the many-particle Hamiltonian in eq 2, the generator $\hat{G}(\mathbf{r})$, as consequence of the principle of stationary action,[5] acts only on the coordinate $\mathbf{r}$. Thus the application of eq 2 yields "dressed" property and current densities for every observable; "dressed" in the sense that the densities include the interaction of the particle at $\mathbf{r}$ with all of the remaining particles in the system. This is exemplified by the definition of the current density $\mathbf{j}_G(\mathbf{r})$ in eq 3

$$\mathbf{j}_G(\mathbf{r}) = (\hbar/2mi)N\int d\tau'\{\psi^*\nabla(\hat{G}(\mathbf{r})\psi) - (\nabla\psi^*)\hat{G}(\mathbf{r})\psi\} \quad (3)$$

The mode of integration over the electronic coordinates denoted by $N\int d\tau'$ is a summation over all spins and an integration over all spatial coordinates, save those denoted by $\mathbf{r}$, the coordinate whose integration is restricted to the open system and where N denotes the number of electrons. When applied to the product $\psi^*\psi$, this mode of integration yields the electron density $\rho(\mathbf{r})$. The symbol $\langle\rangle_\Omega$ denotes the same mode of integration followed by an integration of $\mathbf{r}$ over the open system. Equation 2 is obtained, together with Schrödinger's equation, by restricting his variation of "the Hamilton integral"[6] to a proper open system.

Every choice of $\hat{G}(\mathbf{r})$ yields a theorem:[1,7] $\hat{G}(\mathbf{r}) = \mathbf{p}$, the electronic momentum operator, yields the Ehrenfest force theorem; $\hat{G}(\mathbf{r}) = \mathbf{r}\bullet\mathbf{p}$ yields the virial theorem. The force theorem, eq 4, in which V is the total potential energy operator, is of particular importance

$$\boldsymbol{F}(\Omega) = -\int_\Omega d\mathbf{r}\int d\tau'\psi^*(-\nabla_\mathbf{r}V)\psi = \int_\Omega \boldsymbol{F}(\mathbf{r})d\mathbf{r} = -\oint d\mathbf{S}(\mathbf{r}_s)\cdot\sigma(\mathbf{r}) \quad (4)$$

$\boldsymbol{F}(\Omega)$ is the force exerted on an open system. It is determined by the pressure exerted on every element of its surface $d\mathbf{S}$ by the quantum stress tensor $\sigma(\mathbf{r})$, the momentum current density

$$\sigma(\mathbf{r}) = (\hbar^2/4m)N\int d\tau'\{\psi^*\nabla\nabla\psi - \nabla\psi^*\nabla\psi - \nabla\psi\nabla\psi^* + (\nabla\nabla\psi^*)\psi\} \quad (5)$$

The Ehrenfest force is physically measurable, being the force that is determined in the operation of an atomic force microscope. The force exerted on the probe of the microscope by the sample is a result of the pressure exerted by the sample on each element of the zero-flux surface separating it from the probe.[8] The force density $\mathbf{F}(\mathbf{r})$ is an example of a dressed density: the commutator $(i/\hbar)$ $[\hat{H},\mathbf{p}] = -\nabla_\mathbf{r}V$, is the force exerted on the electron at $\mathbf{r}$ by the remaining particles, all in some fixed position, and when multiplied by $\psi^*\psi$ and averaged by the above recipe, it yields the force exerted on the electron density at $\mathbf{r}$, averaged over the motions of the remaining electrons.

The atomic virial theorem is given in eq 6:

$$-2T(\Omega) = v_b(\Omega) + v_s(\Omega) = v(\Omega) \quad (6)$$

where $v_b(\Omega)$ is the virial of the Ehrenfest forces acting within the atom, the subscript in this case denoting the atomic basin, and $v_s(\Omega)$ is the virial of the same forces acting in the atomic surface. For an internuclear separation R at which the Hellmann−Feynman forces on the nuclei vanish, the total virial $v(\Omega)$ equals the potential energy.

The mechanics of an open system also yields a local statement of each atomic theorem. The local form of the Ehrenfest force theorem for a stationary state is

$$\mathbf{F}(\mathbf{r}) = -\nabla\cdot\sigma(\mathbf{r}) \quad (7)$$

while for the virial theorem the local expression is

$$(\hbar^2/4m)\nabla^2\rho(\mathbf{r}) = 2G(\mathbf{r}) + v(\mathbf{r}) \quad (8)$$

where $G(\mathbf{r})$ is the positive definite form of the kinetic energy density and $v(\mathbf{r}) = -\mathbf{r}\cdot\nabla\cdot\sigma(\mathbf{r}) + \nabla\cdot(\mathbf{r}\cdot\sigma(\mathbf{r}))$ is the virial field. The virial field integrates to the virial v and is thus a representation of the potential energy density. It has been shown to be homeomorphic with the electron density,[9] leading to the observation that the nuclei of a pair of bonded atoms are linked by both bond and virial paths, the line of maximum density representing a line of maximally negative potential energy. The sign of $\nabla^2\rho_b$ determines whether the kinetic or potential energy densities dominate a given interaction, relative to their two-to-one weighting in the virial theorem. It is useful to define an energy density $H(\mathbf{r}) = G(\mathbf{r}) + v(\mathbf{r})$ whose value at the bond critical point H_b determines which contribution dominates the energy density in the vicinity of the critical point.[10] The value of the virial field at the same point, $v_b = Tr\sigma(\mathbf{r})$, provides a measure of the potential energy density.

Atomic Properties.[1] The atomic charge $q(A) = Z_A - N(A)$ is the difference between the nuclear charge of atom A and its average electron population, the expectation value of the number operator over the atomic basin. The atomic first moment $\mathbf{M}(A)$ is obtained by averaging the operator $-e\mathbf{r}_A$ with origin at nucleus A over the density of atom A. The molecular dipole moment can be expressed as $\mu = \mu_{CT} + \mu_{AP}$; μ_{CT} and μ_{AP} are respectively, the contributions from the interatomic charge transfer and from the atomic dipolar polarizations. For a neutral diatomic, $\mu_{CT} = q(A)\mathbf{R}$ with $\mathbf{R} = \mathbf{X}_A - \mathbf{X}_B$ and $\mu_{AP} = \mathbf{M}(A) + \mathbf{M}(B)$. The two contributions, in general, oppose one another. The atomic quadrupolar polarization with respect to the molecular axis z, the quantity $Q_{zz}(A)$, is obtained by averaging $-e(3z_A^2 - r_A^2)$ over the density of the atom. The perpendicular components are related by $Q_{xx}(A) = Q_{yy}(A) = -{}^1/_2Q_{zz}(A)$, as required for a traceless tensor. The sign of $Q_{zz}(A)$ determines whether electronic charge is accumulated along the molecular axis within the basin of the atom, $(Q_{zz}(A) < 0)$, or concentrated in a a torus-like accumulation about the axis, $(Q_{zz}(A) > 0)$.

Harpoon Mechanism and the Formation of LiF. The $^1\Sigma^+$ ground states of alkali halide molecules MX, such as LiF, exhibit the characteristics of a closed-shell interaction between ions with charges approaching $\pm 1e$.[1] Since these same molecules dissociate into ground state neutral atoms, the adiabatic potential energy curves representing the separate "ionic" and "covalent" $^1\Sigma^+$ states must cross in the zeroth-order approximation.[11] One can estimate R_c, the internuclear separation at which the crossing occurs, by equating the energy required to ionize the atom M that is in excess of the energy released, as determined by the electron affinity of X, to the electrostatic energy of attraction resulting from the formation of the ion pair. Since the ionization potential of M is only slightly larger than the electron affinity of X, this leads one to anticipate large crossing radii. Using experimental values for the relevant quantities in LiF, one

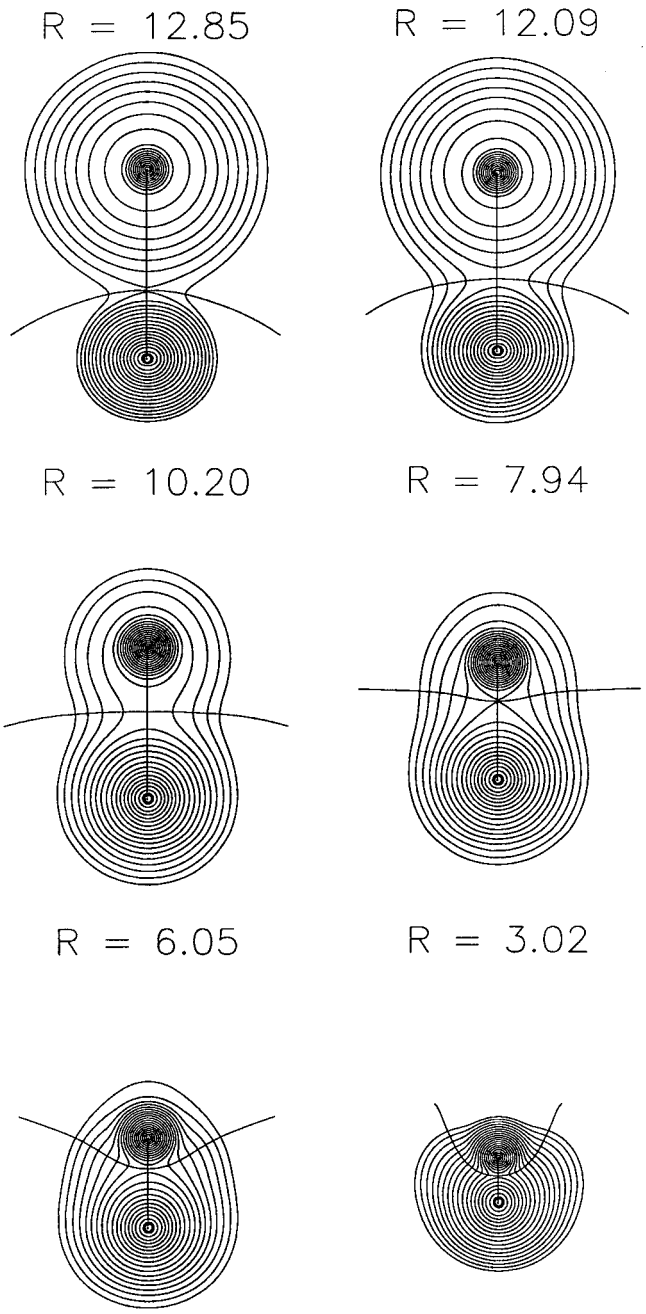

Figure 1. Contour maps of the electron density depicting the evolution of the molecular density distribution and the interatomic surface of LiF into its equilibrium form, as a function of the internuclear separation *R*. Li is the upper atom here and in Figure 4. The bond CP is located at the intersection of the bond path with the profile of the interatomic surface. The density of the F atom at $R = 12.85$ au exhibits a quadrupolar polarization corresponding to a deficiency of density along the axis of approach consistent with the valence state configuration $2p_\sigma^1\ 2p_\pi^4$. The density contours in this and the remaining figures increase inward in the progression $2^n \times 10^{-5}$, with $n = 1, 2, 3, ..., 20$, the highest contour having the value 10.49 au.

obtains $R_c = 13.7$ au.[12] The mixing of the two states is small at these large distances, and hence the electron transfer is predicted to be an abrupt process, occurring at a large separation, the so-called harpoon mechanism.[13] One anticipates that of the molecules studied here, the formation of LiF will exhibit the most striking changes in its electron density distribution.

Both the curve crossing and the large correlation contribution to the electron affinity of the halogens contribute to the difficulty of obtaining a proper description of the formation of LiF,[12] and

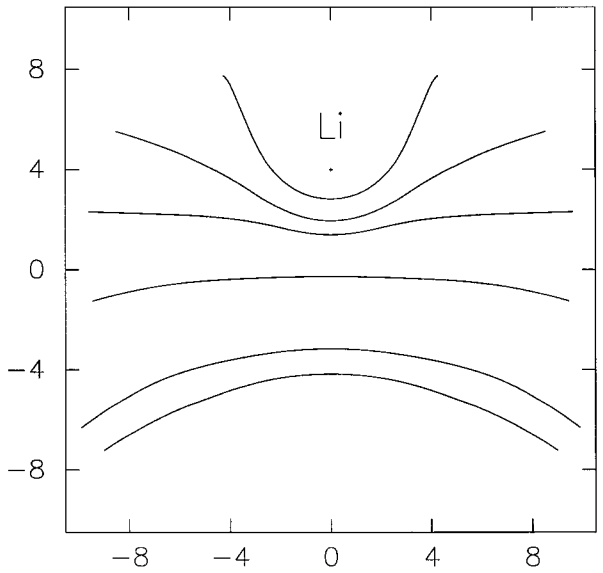

Figure 2. The evolution of the interatomic surface in LiF portrayed with respect to a stationary Li nucleus for the same values of *R* given in Figure 1.

no single-referenced-based method is satisfactory.[12,14] The calculations reported here use the multireference configuration interaction (MRCI) given in GAMESS[15] with an active space comprising the 3σ, 4σ, 1π, and 2π orbitals that are used to describe all possible single and double excitations. The basis set consisted of the contraction (10s,6p,4d)/[5s,3p,2d] for both F[16] and Li.[17] The calculated equilibrium separation and dissociation energy are: $R_e = 3.024$ au, $D_e = 5.68$ ev with corresponding experimental values[12] of 2.96 au and 6.00 ev.

Metamorphism of the Density in LiF. The dramatic change in the morphology of $\rho(\mathbf{r})$ encountered in the formation of LiF and the resulting changes in the atomic boundaries are pictured in Figure 1. Note the disparity in the atomic sizes for large *R* and how this disparity is reversed at the equilibrium separation R_e. Figure 2 summarizes the changes in the shape of the interatomic surface and its advance toward the Li nucleus that accompanies the transfer of electron density from Li to F. The operation of the "harpoon" mechanism is made most evident in the very abrupt increase in the atomic charge on Li, q(Li), which is initiated at ~12 au and attains its equilibrium value of 0.94e by 10 au, Figure 3a. The same abrupt character of the charge transfer process is also evident in the sharp and sudden increase in the value of the molecular dipole moment μ to a maximum of 24.2 D at $R = 10.2$ au, which then declines to its equilibrium value of 6.38 D (6.28 exp[12]), Figure 3b. Essentially the whole of the dipole moment is accounted for by the charge transfer component μ_{CT}. The molecular value of μ is slightly reduced from μ_{CT} by a small polarization of the density of the fluorine atom in a direction counter to the direction of charge transfer. The atomic polarization of the tightly bound density of the lithium ion makes only a negligible contribution to μ.

There is a monotonic increase in the values of ρ_b and $\nabla^2\rho_b$ for values of $R < 8$ au following the transfer of charge, Figure 3c, and at R_e they attain values characteristic of a closed-shell interaction, with $\rho_b < 0.1$ au and $\nabla^2\rho_b > 0$, Table 1. The value of $\nabla^2\rho_b$ becomes negative over a small range of separations around $R = 9$ au (see insert in Figure 3c) that arises from the last remnant of the valence shell of charge concentration of the Li atom being found in the vicinity of the critical point, a point made clear in the discussion of the Laplacian distribution. The steep rise in $\nabla^2\rho_b$ occurs after the completion of charge transfer.

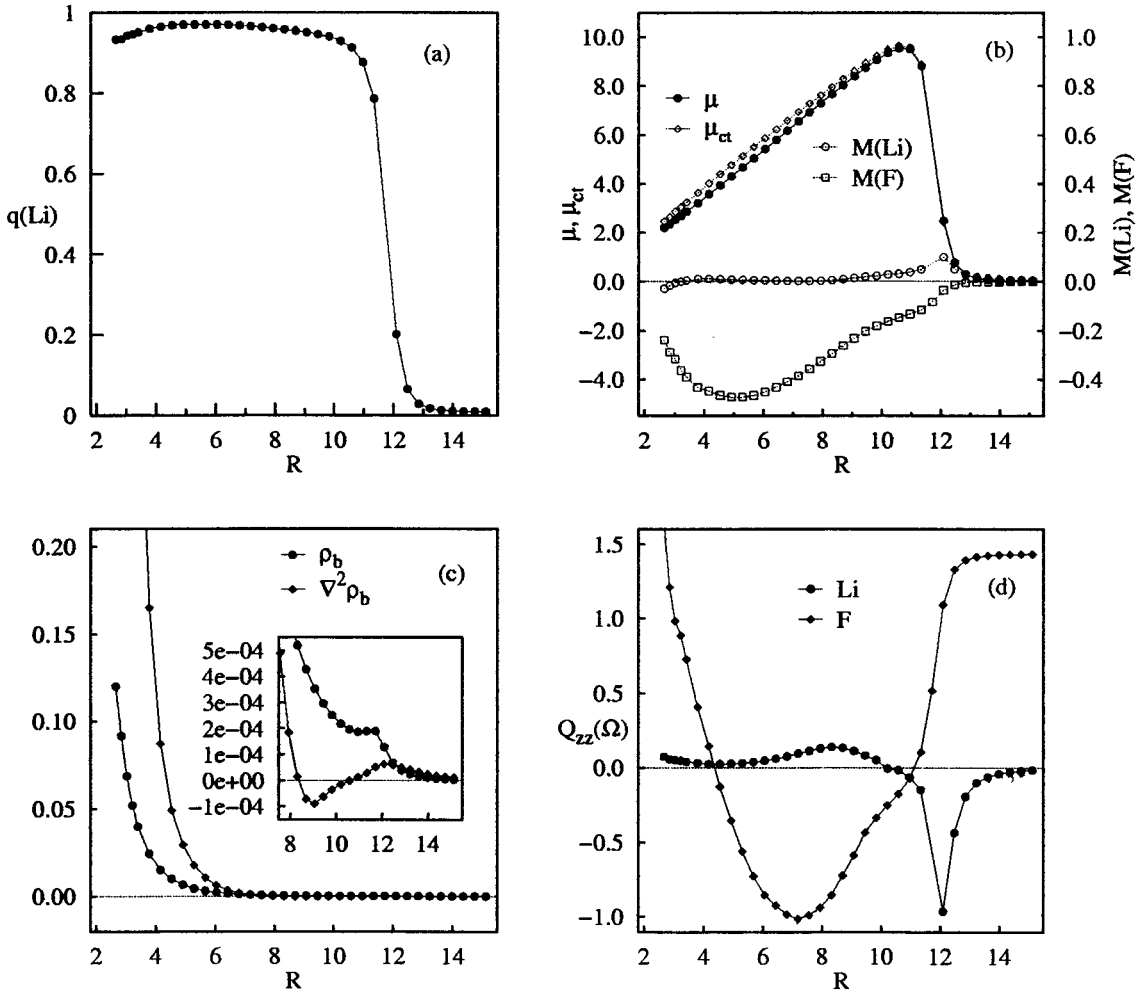

Figure 3. Atomic and bond properties of LiF as a function of R: (a) the charge on Li, q(Li); (b) the molecular dipole moment $\boldsymbol{\mu}$, its charge transfer $\boldsymbol{\mu}_{ct}$ and the atomic polarization components $\mathbf{M}(\Omega)$, the latter being plotted versus a reduced scale; (c) density and its Laplacian at bond CP, ρ_b, and $\nabla^2\rho_b$; (d) atomic quadrupole polarizations with respect to the molecular axis, $Q_{zz}(\Omega)$.

TABLE 1: Critical Point Data (in atomic units) for Equilibrium Geometries[a]

AB	R_e	ρ_b	$\nabla^2\rho_b$	G_b	H_b	ϑ_b
LiF	3.024	0.0689	+0.6383	0.1455	+0.0140	−0.1315
H_2	1.402	0.2704	−1.2546	0.0106	−0.3243	−0.3349
N_2	2.069	0.7117	−3.0847	0.6381	−1.4093	−2.0475
CO	2.131	0.5040	+0.6657	1.1564	−0.9900	−2.1463
Ar_2	7.050	0.0032	+0.0130	0.0025	+0.0008	−0.0017

[a] Results for H_2, N_2, and CO are from QCISD SCVS using the 6-311++G(2df,2dp) basis. The results for LiF and Ar_2 are as given in the text.

It is a result of density being increasingly displaced from the region of overlap between what are now two closed-shell ions and being accumulated within the basin of the fluorine atom. As a consequence, the axial curvature of the density at the bond CP dominates the sign of $\nabla^2\rho_b$, and from the expression for the local virial theorem, eq 8, the interaction in the region of the bond CP is dominated by a local increase in the kinetic energy density. The kinetic energy per electron at R_e is in excess of unity, $G(r_b)/\rho(r_b) = 2.1$ and the energy density assumes a positive value, with $H_b = +0.014$ au. These characteristics are the opposite to those found in a shared interaction and the LiF molecule achieves its stability through the electron density transferred to and accumulated within the basin of the F atom,[1] a point discussed below.

The nonspherical nature of the fluorine density upon the initial approach of the atoms is evident in Figure 1. There is a pronounced quadrupolar polarization of fluorine, corresponding to a depletion of its density along the axis of approach, as reflected in the large limiting positive value of $Q_{zz}(F) = 1.4$ au at $R = 14$ au, Figure 3d. The creation of the axial field caused by the approach of the Li atom partially removes the degeneracy of the atomic states associated with the ^2P term of the F atom resulting in the $M_L = 0$ component having the lowest energy, the component corresponding to a configuration with the single vacancy in the $2p\sigma$ orbital. This is the same component previously used in the construction of density difference maps for molecules formed from ground state fluorine atoms. It was shown that density difference maps yield consistent patterns of charge reorganization when referenced so as to reflect the proper mixture of atomic states that is obtained upon dissociation of the molecule.[18] Molecules do not dissociate into atoms with sphericalized densities, but rather into valence states corresponding to a mixture of the lowest energy states as determined in the limit of vanishing λ, the quantum number governing the component of electronic angular momentum about the axis, as exemplified by the density for the fluorine atom at $R = 12.9$ au, Figure 1.

The charge transfer that is initiated at 12 au causes a rapid decrease in $Q_{zz}(F)$ and the quadrupole moment vanishes between 11 and 10 au corresponding, in the orbital model, to the transferred density filling the $2p_\sigma$ hole on the F atom, Figure 3d. The continued approach of what is now a positively charged Li atom causes a marked accumulation of density along the

molecular axis within the basin of the F atom, as is also evident from the total density map for $R = 7.94$ au (Figure 1), and $Q_{zz}(F)$ becomes negative. However, the further approach of the closed-shell Li core results in a removal of density from along the axis and causes $Q_{zz}(F)$ to increase to $+0.98$ au at the equilibrium separation. The value of $Q_{zz}(Li) = 0$ for large R, as anticipated for an S state atom, but decreases precipitously just before the electron is transferred, a result of valence density being accumulated along the axis prior to its transfer to the F atom. The value becomes small and positive following the charge transfer, and the Li atom, which consists primarily of a tight core density, exhibits only a slight positive quadrupolar polarization at R_e with $Q_{zz}(Li) = 0.05$ au.

The Laplacian of ρ and Electron Localization. The Laplacian of the electron density determines where electron density is locally concentrated, $\nabla^2\rho(\mathbf{r}) < 0$, and locally depleted, $\nabla^2\rho(\mathbf{r}) > 0$. It is convenient to discuss the topology in terms of $L(\mathbf{r}) = -\nabla^2\rho(\mathbf{r})$, a maximum in $L(\mathbf{r})$ corresponding to a maximum concentration of electronic charge. For a free atom $L(\mathbf{r})$ exhibits shells of alternating charge concentration and charge depletion that mimic atomic shell structure, each shell being represented by a pair of such regions, the outer shell with $L(\mathbf{r}) > 0$, being referred to as the valence shell of charge concentration (VSCC). The shell structure persists for an atom in a molecule, but the surface over which the density is maximally concentrated in the VSCC of a free atom is distorted by the formation of local maxima or charge concentrations (CCs), minima and saddles on its surface in response to the bonded interactions. It is the topology exhibited by the CCs formed in the VSCC of the ligand-bearing atom that faithfully maps onto the number and arrangement of the bonded and nonbonded electron pair domains postulated in VSEPR model of molecular geometry.[1,19]

A homeomorphism has been demonstrated between the Laplacians of the electron density and of the conditional pair density when the latter density is sampled by the positioning of a pair of reference electrons.[20] The conditional pair density approaches the electron density in those regions of space removed from a position that localizes the pair of reference electrons. Under these conditions, the maxima in the negative of the Laplacian of the conditional pair density, which now closely approximate the CCs of $L(\mathbf{r})$, indicate where the remaining pairs are most likely to be found. This homeomorphism approaches an isomorphic mapping of one field onto the other, as the reference electron pair becomes increasingly localized to a given region of space. Thus the CCs displayed in $L(\mathbf{r})$ signify the presence of spatial regions of partial pair condensation, regions with greater than average probabilities of occupation by a single pair of electrons, and $L(\mathbf{r})$ provides a mapping of the essential aspects of electron pairing determined in six-dimensional space, onto the real space of the density.

The changing patterns in the function $L(\mathbf{r})$ for the formation of LiF are displayed in Figure 4. Of particular importance is the change in the shell structure observed for the Li atom. The homeomorphism between the Laplacians of the density and of the conditional pair density approaches an isomorphism for the free atoms, a situation approached for $R > 12$ au. At these separations, $L(\mathbf{r})$ indicates the presence of two quantum shells for each atom, the structure for fluorine being very contracted compared to that for lithium. However, between $R = 12$ and 10 au, the range of R values over which the electron is transferred, the outer shell of charge depletion on the lithium atom vanishes and its VSCC is reduced to a small bonded charge concentration. By 8 au even this remnant of the VSCC of lithium is found within the basin of the fluorine atom and $L(\mathbf{r})$ for lithium exhibits a shell structure consistent with that for a lithium ion.

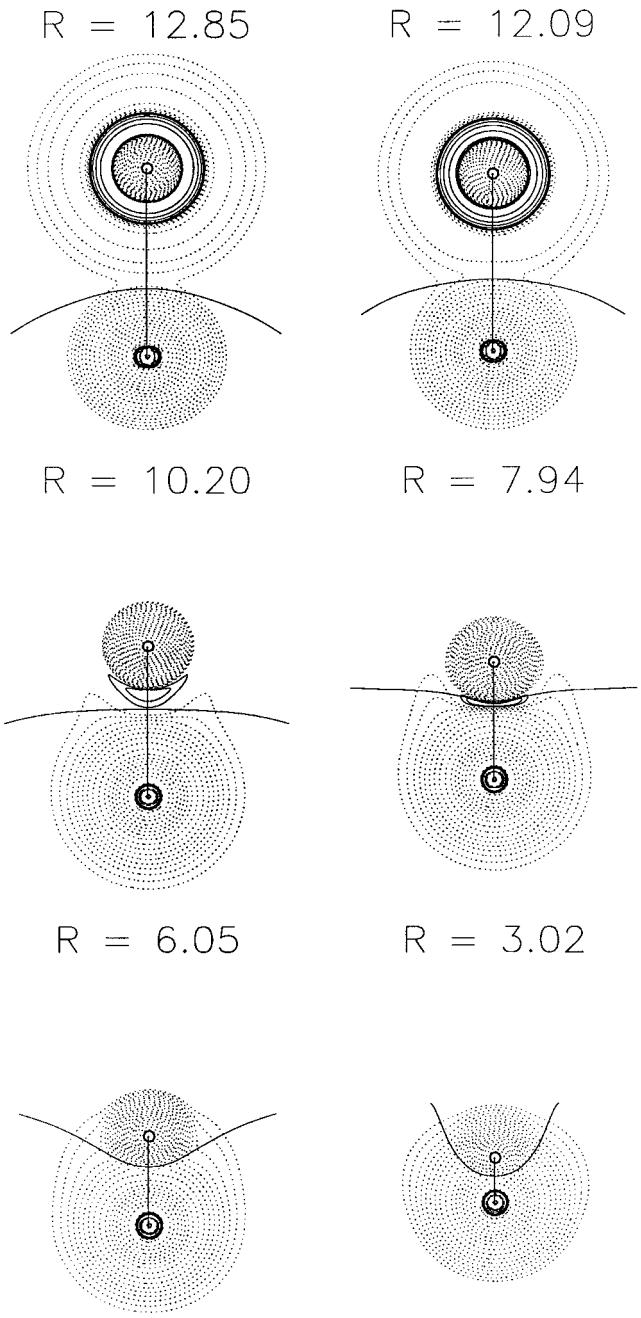

Figure 4. Laplacian of the electron density for LiF as a function of R. Solid contours denote concentration of electronic charge, $L(\mathbf{r}) > 0$, dashed contours a depletion, $L(\mathbf{r}) < 0$. Each atom initially exhibits two quantum shells, an inner and a valence shell, the radii of the shells being much reduced for F compared to Li. At R_e, $L(\mathbf{r})$ for Li, indicates the presence of only an inner shell. Absolute values of contours are the same as those used to display the density.

The VSCC for the fluorine atom exhibits a torus of charge concentration for large separations, consistent with the pairing of electrons described by the free atom configuration $2p_\sigma^1 2p_\pi^4$ and reflected in the behavior of $Q_{zz}(F)$ for $R > 12$ au, Figure 3d. The transfer of charge that occurs between $R = 12$ and 10 au results in the torus becoming less pronounced, and the VSCC assumes a more nearly spherical distribution consistent with the filling of the $2p_\sigma$ orbital to yield a closed-shell fluorine anion. In addition, the torus is displaced toward the nonbonded side of the atom, and at 3.4 au it collapses into a single nonbonded axial maximum. At $R = 3.2$ au a bonded maximum appears as

well, the presence of axial bonded and nonbonded maxima linked by a torus of (2,0) CPs, persisting on through to the equilibrium separation, a pattern typical of second and third row atoms with an intact VSCC.

The Formation of H_2 and N_2: Shared Interactions. The molecules H_2 and N_2 both result from the combination of atoms in open shell S states, ^2S and ^4S, respectively, and CI is required to obtain the correct dissociation limits. The hydrogen molecule has been extensively studied, Kolos et al.[21] having determined the dissociation energies for all of the isotopic species of this molecule beyond the Born−Oppenheimer limit. The quadratic configuration interaction method, including all singles and doubles, (QCISD) of Pople and Head-Gordon[22] was employed for H_2, together with the 6-311++G(2pd) basis using the program *Gaussian 94*.[23] This was coupled with a self-consistent scaling of the electronic coordinates (SCVS), as required to satisfy the virial theorem. The $^1\Sigma_g^+$ ground state of H_2 is calculated to have $R_e = 1.402$ au and $D_e = 4.699$ ev, the corresponding experimental values[24] being 1.401 au and 4.75 ev.

A number of calculations of the potential energy curves for the lowest states of N_2 have appeared over the past two decades.[25−29] They have demonstrated that a high level of electron correlation is required for the prediction of its spectroscopic constants, an MRCI method proving particularly effective. Accordingly, the wave functions reported here use a (10s,6p,4d)/[5s,3p,2d] basis set[17] in a MRCI that included all single and double excitations of the configurations obtained from an active space comprising the 5σ, 1π, 2π, and 6σ orbitals. The $^1\Sigma_g^+$ ground state is calculated to have $R_e = 2.112$ au and $D_e = 9.020$ ev, the respective experimental values[30] being 2.074 au and 9.892 ev.

The changing topology of the density encountered in the formation of the shared interactions in H_2 and N_2, Figure 5, lies at the opposite extreme from that for the ionic closed-shell interaction encountered in the formation of LiF. The initially spherical atomic densities merge upon their mutual approach and density is increasingly accumulated in the internuclear region, as evidenced by the steep rise in ρ_b for both molecules, Figure 6a. The differing mechanics of the closed-shell and shared interactions are brought to the fore in the behavior of $\nabla^2\rho_b$, as well as of ρ_b. After a slight initial rise for $R > 4$ au in the case of N_2, $\nabla^2\rho_b$ undergoes a steep decline and subsequently becomes negative for both molecules, the equilibrium values being given in Table 1 for QCISD SCVS wave functions obtained using a large basis set for N_2 and CO, and H_2. While the values for the large basis set do not differ greatly from those obtained using the smaller basis sets, the data in Table 1 provide a uniform basis for a comparison of CP properties. Unlike a closed-shell interaction, not only are all three curvatures of the density large in magnitude, but $\nabla^2\rho_b < 0$ as a result of the dominance of the perpendicular contractions of the density toward the bond path. The local virial theorem, eq 8, thus determines that the interactions are stabilized by the accumulation of potential energy density in the internuclear region and one finds that the energy density H_b is negative for both H_2 and N_2, the values of the virial field v_b being more negative still, Table 1. The kinetic energy per electron at the bond critical point is less than unity for these interactions, $G_b/\rho_b = 0.04$ au for H_2 and 0.90 au for N_2, compared to the value of 2.1 au for LiF. These molecules are stabilized by a lowering of the potential energy resulting from the sharing of the density accumulated between the nuclei.

In the case of H_2, the increasing accumulation of density in the internuclear region is reflected in an initial increase in the atomic first moment, Figure 6b, corresponding to an inward polarization of the density for $R > 2.4$ au. However, for a further decrease in R, the direction of the atomic first moment is reversed and the atomic polarization of H, like N in N_2, is directed toward its nonbonded region. This effect is determined not by a decrease in the transfer of density to the bonding region as R is decreased, but by the decrease in the bonded radius of the atom (the distance from the nucleus to the bond CP) compared to its nonbonded radius (nonbonded distance from nucleus to 0.001 au density contour, the van der Waals size[1]). Reference to the total densities displayed in Figure 5, shows that for $R < 9.5$ au in the case of N_2, the nonbonded radius

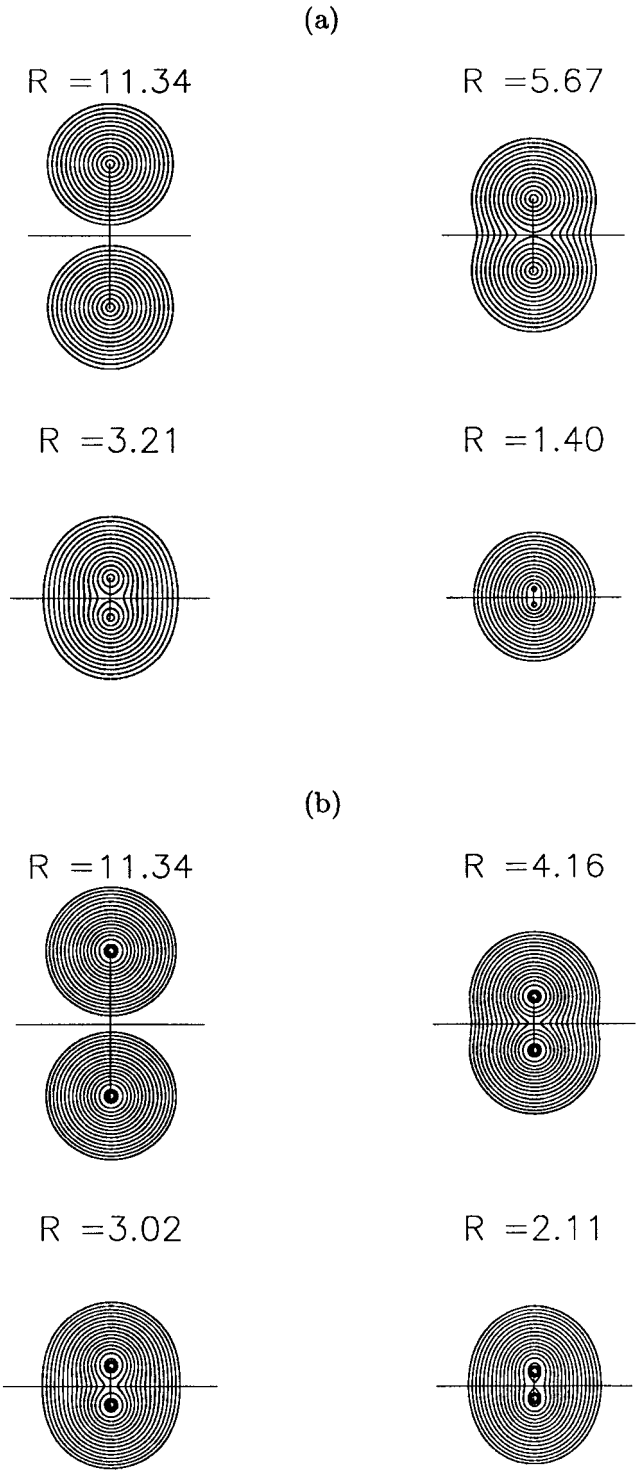

Figure 5. The evolution of the molecular density distributions for H_2 in (a) and N_2 in (b).

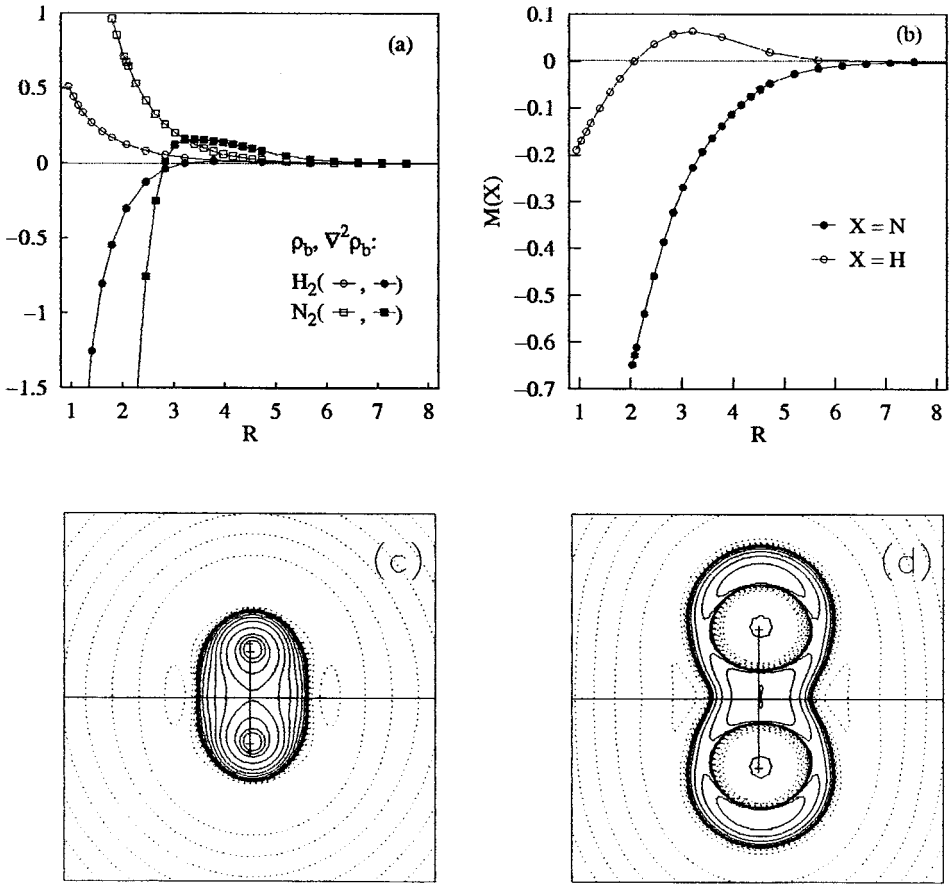

Figure 6. Atomic and bond properties as a function of R for H_2 and N_2: (a) density and its Laplacian at bond CP; (b) atomic polarizations $\mathbf{M}(\Omega)$; (c) and (d) equilibrium Laplacian distributions for H_2 and N_2, respectively.

exceeds the bonded one and the contribution of the nonbonded density to **M**(N) will dominate because of its greater spatial extent and consequent greater weighting of the dipole operator. Both molecules exhibit positive quadrupole moments, and the atomic contributions to the electronic portion of this moment correspond to a removal of density from along the molecular axis and to its accumulation about the axis. This behavior of the first and second atomic moments is characteristic of all the homonuclear diatomics formed from the second-row atoms.[1]

The Laplacian distribution for the H_2 molecule exhibits the essential features associated with the formation of a shared interaction: the VSCC encompassing each proton polarizes toward the approaching atom and, for $R < 3.21$ au, they merge to yield a single region of charge concentration contiguous over the basins of both atoms, Figure 6c. This is a result of the dominance of the perpendicular contractions of the density toward the bond path as monitored by the increasingly negative values of $\nabla^2\rho_b$. Similar behavior is found for N_2 where the VSCCs merge for $R \sim 3.2$ au and form a charge concentration that is contiguous over the valence regions of both atoms, Figure 6d. This behavior is common to homonuclear diatomics from the second row. Each VSCC exhibits axial bonded and nonbonded CCs linked by a torus of (2,0) CPs, the same pattern found for a fluorine in LiF. In LiF however, the VSCC is localized within the fluorine basin and $\nabla^2\rho_b > 0$. In terms of the local virial theorem, eq 8, it is the shared concentration of charge in H_2 and N_2, as displayed in Figure 6c and d, that is responsible for the lowering of the potential energy and for the bonding found in shared interactions.

The changing structure within a VSCC of a nitrogen atom gives a portrayal of the behavior of the pair density that accompanies bonding.[20] Initially, the partial condensation of the pair density results in the formation of a torus of (2,−2) CCs, which is increasingly displaced toward the nonbonded region and which eventually collapses at $R \sim 3.4$ au into the axial nonbonded CC found in the equilibrium distribution. The bonded CC arises from the bifurcation of an axial (3,+1) CP into the bonded (3,−3) CP and a torus of (2,0) CPs at $R \sim 3.8$ au to yield the pattern of pairing consistent with the Lewis model: a CC denoting a nonbonded pair on each atom and two bonded CCs that are shown by the pair density to refer to the same set of coupled electron pairs.[20] The behavior of the pair density on bond formation has been studied by Silvi and co-workers[31] through a study of the dynamics of the topology displayed by the electron localization function (ELF) of Becke and Edgecombe,[32] the appearance and disappearance of bonded pairs appearing as catastrophic changes in the form of ELF. Ponec and Ponec and Carbo-Dorca[33] have studied the fluctuation in the electron population associated with a given set of orbitals when the hydrogen molecule is dissociated, the orbitals being chosen through a unitary transformation so as to minimize the bond fluctuations. The sum of the bond fluctuations determined in this manner exhibits a sharp maximum when the bond is stretched to 1.25 Å, a point discussed in detail by the authors.

Formation of CO: A Shared Polar Interaction. The importance of electron correlation in the calculation of the spectroscopic constants of CO is well documented, most recently by Peterson and Dunning.[34] The wave functions reported here were obtained using a Dunning (9s,4p1d)/[3s,2p,1d]basis set[35] in an MRCI[15] using all of the possible single and double excitations obtained from the configurations arising from an active space

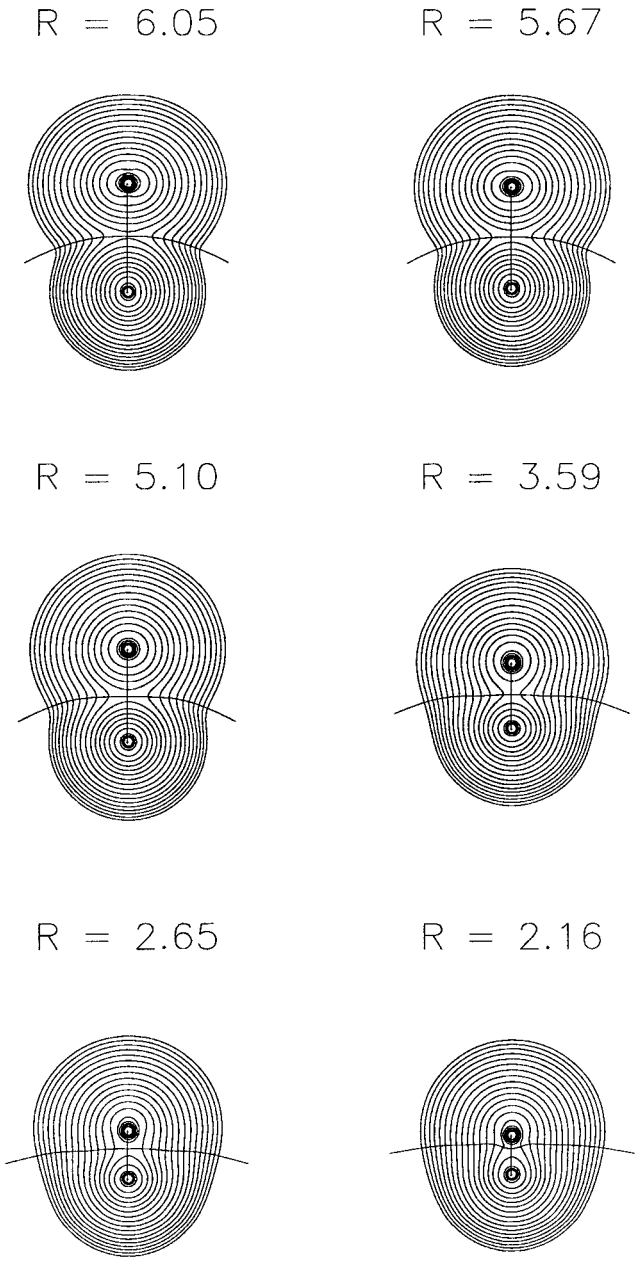

Figure 7. Evolution of the molecular density distribution and the interatomic surface for CO. Note the increase in the nonbonded radius of C, the upper atom, as R is decreased.

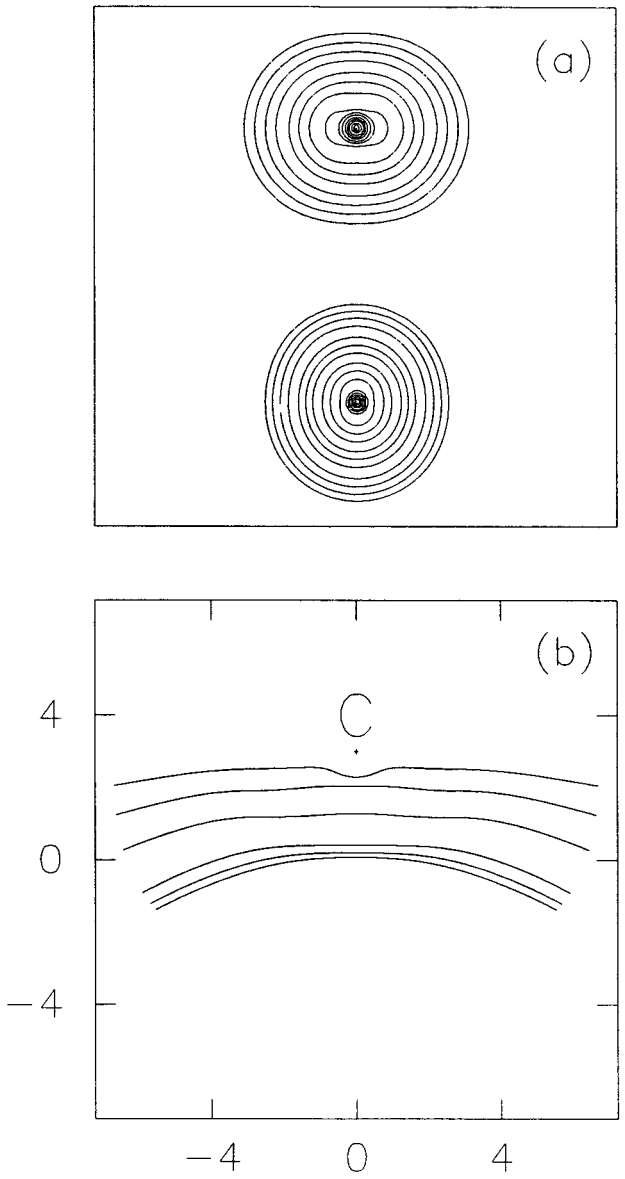

Figure 8. (a) The electron density distribution of CO at $R = 9.3$ au showing the distinct quadrupolar polarizations of the atomic densities with respect to the molecular axis, oxygen being polarized along the axis and carbon being polarized about the axis. (b) The evolution of the interatomic surface in CO portrayed with respect to a stationary carbon nucleus. Note how its equilibrium form reflects the boundary of the inner core density on carbon.

comprising the valence orbitals, this size active space, and basis set exhausting our computing facilities. The calculated values of R_e and D_e are in fair agreement with experiment, the respective values (experimental values[30] bracketed) being 2.165 au (2.138 au) and 10.4 ev (11.18 ev). The calculations failed to converge for $R > 6.2$ au, a problem that was overcome through removal of the 2s orbitals from the active space. The calculations with this reduced active space were continued to large R to ensure that the limiting atomic state convergence obtained at $R < 6.2$ au was correct.

The changing morphology of the electron density accompanying the formation of CO is depicted in Figure 7. The molecule is formed from atoms in states arising from ^{3}P terms, and the open shell nature of the densities of the initial states of the interacting atoms is evident for $R = 6$ au where both exhibit marked quadrupolar polarizations, axial for oxygen and torus-like for carbon, the same pattern of polarizations found at $R = 9.3$ au using the reduced active space, Figure 8 a. The states of the ^{3}P term that participate in the formation of the $^1\Sigma^+$ ground state of CO are those with $M_L = M_S = 0$ for both atoms. For carbon, with the configuration $2p^2$, there is an equal mixing of the state with occupation $\pi_+\alpha,\pi_-\beta$ with the one obtained by a spin interchange, where the quantization is with respect to the molecular axis. This mixing corresponds to the open-shell occupation $p_\sigma^0 p_\pi^2$, thereby accounting for the torus-like polarization of the carbon atom density. The electron configuration of oxygen is $2p^4$ and, because of the particle−hole formalism, the equivalent mixing of states for oxygen corresponds to the initially perturbed atom possessing the open shell occupation $p_\sigma^2 p_\pi^2$. Thus the initial valence states of the atoms are both nonspherical, the oxygen possessing a depleted π density and the carbon a depleted σ density, Figure 8a.

The interatomic charge transfer of 1.2 e occurring in the formation of CO is greater than that encountered in the formation of LiF, but the resulting charged atoms retain valence density

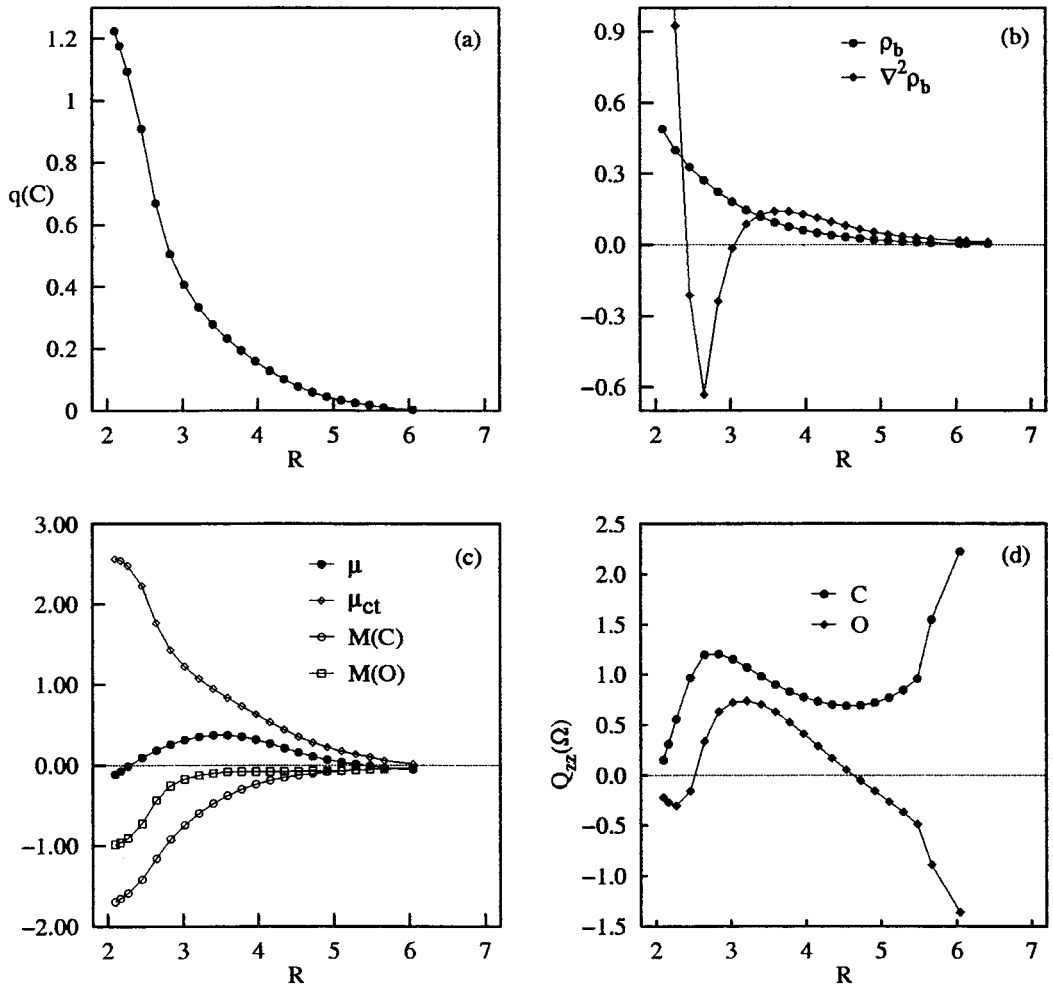

Figure 9. Atomic and bond properties of CO as a function of R: (a) charge on carbon, q(C); (b) density and its Laplacian at bond CP; (c) molecular dipole moment $\boldsymbol{\mu}$, its charge transfer $\boldsymbol{\mu}_{ct}$ and atomic polarization components $\mathbf{M}(\Omega)$; (d) atomic quadrupole polarizations with respect to the molecular axis, $Q_{zz}(\Omega)$.

and their charge distributions do not approach those of closed-shell ions. Thus the bonding, while polar, exhibits none of the characteristics of an ionic interaction. The transfer of charge occurs primarily within the internuclear region, the advance of the interatomic surface toward the carbon nucleus accompanying the decrease in R being apparent in Figure 8b. Initially, the CP is positioned so as to yield a larger bonded radius for carbon than for oxygen, 3.37 compared to 3.01 au at $R = 6.4$ au, as anticipated on the basis of the relative atomic sizes. However, at R_e, the bonded radii are 0.69 and 1.41 au for carbon and oxygen, respectively. It is important to note that the nonbonded radius of carbon, the axial distance from the nucleus to the 0.001 au density contour, actually increases upon bonding, from 3.34 au at $R = 6.4$ au to 3.72 au at R_e. The corresponding radius of the oxygen atom undergoes a small decrease, from 3.30 au to 3.18 au for the same separations. This accumulation of nonbonded density on the carbon atom, apparent in the total density distributions, has a very dramatic effect upon all of the molecular properties, particularly the dipole moment. It is clear that the reorganization of density accompanying bonding corresponds to the partial filling of the respective p_σ and p_π vacancies that are present in the densities of the carbon and oxygen atoms upon their initial approach.

The equilibrium density distribution and the form exhibited by its interatomic surface, Figure 8b, indicate that the 1.2 e transferred to oxygen, Figure 9a, corresponds to the essentially complete transfer of the valence density from the bonded side of the carbon atom, the equilibrium interatomic surface exhibiting a bulge caused by its approach to the core of the carbon atom. There is a monotonic and substantial increase in ρ_b characteristic of a shared interaction, but $\nabla^2\rho_b$ exhibits more complex behavior, Figure 9b. Initially the bond CP is approximately equally spaced between the two nuclei and the positive curvature dominates because of the vacancy in the sigma density on carbon. However, the transfer of charge results in the eventual dominance of the perpendicular curvatures, and $\nabla^2\rho_b$ becomes negative corresponding to the contraction of the density toward the bond path and to its accumulation in the internuclear region, as evidenced by the associated increase in ρ_b. These are the characteristics of a shared interaction. This behavior persists for a further decrease in R, but as the bond CP approaches the steeply rising density of the carbon core that is exposed as a result of the further transfer of charge, the positive curvature again dominates the interaction. The sign of $\nabla^2\rho_b$ can be positive or negative for a polar interaction, depending on the position of the bond CP relative to the core of the electropositive atom, as is evident from the very steep rise in its value for CO just before the equilibrium separation is attained. Unlike a closed-shell interaction for which $\nabla^2\rho_b$ is also positive, the magnitudes of the contributing curvatures are large for a polar interaction, as is the value of ρ_b, indicating that a significant amount of electron density is accumulated and shared between the two atoms. Thus the energy density H_b as well as the virial density v_b is negative, with values similar to

those obtained for N_2, Table 1 which gives results for a high level of theory.

The magnitude of the dipole moment of CO is predicted to be small, 0.074 au, and in the direction C^-O^+, in agreement with experiment, the latter value being 0.0481 au.[36] The direction of the dipole is contrary to that anticipated on the basis of the direction of the interatomic charge transfer, but readily accounted for in terms of the polarizations of the atomic distributions. Figure 9c illustrates how the charge transfer contribution to the dipole is eventually overwhelmed at R_e by the accompanying counter polarizations of the atomic densities, particularly the contribution from carbon. This expansion of the density into the nonbonded region of the carbon atom in response to the negative field exerted by the approaching oxygen is, as noted above, evident in the displays of the molecular density distributions and corresponds to the filling of the $2p_\sigma$ vacancy initially present on the carbon atom.

The atomic quadrupole moments provide another complementary view of the dominant changes in ρ that accompany the formation of CO, Figure 9d. The opposing quadrupole polarizations of the two atomic densities found for the initial valence states of the interacting atoms are evident in $Q_{zz}(C) > 0$ and $Q_{zz}(O) < 0$, with the overall moment being dominated by the carbon contribution. The interatomic charge transfer results in a decrease in the magnitudes of both contributions with, $Q_{zz}(O)$ changing sign at $R \sim 4.5$ au, the same point at which $Q_{zz}(C)$ attains its minimum value. The further transfer of density from oxygen to carbon enhances the π contributions to both moments, the final distributions exhibiting only small quadrupolar polarizations, as the original orbital vacancies are obliterated.

The behavior of the Laplacian distributions, Figure 10, demonstrates that the distinctive changes in the atomic polarizations encountered during bond formation are a consequence of the changes in the pairing of the valence electrons. For all separations, the VSCC of oxygen exhibits two axial CCs, one bonded the other nonbonded, as anticipated for the configuration $p_\sigma^2 p_\pi^2$. The VSCC of carbon, on the other hand, exhibits a torus of CC for large separations in line with the configuration $p_\sigma^0 p_\pi^2$. This torus, initially encircling the axis at the position of the carbon nucleus, is pushed progressively into the nonbonded region of the atom, its radius diminishing until at $R \sim 4.1$ au, it collapses into a nonbonded CC, nearly simultaneous with the appearance of a bonded CC. At R_e, the pattern of partial pair condensation found in CO is identical to that found in the isoelectronic N_2, with each atom exhibiting bonded and nonbonded CCs, with the nonbonded CC on carbon being particularly pronounced.

Formation of Ar_2: a van der Waals Interaction. The $^1\Sigma_g^+$ ground state of Ar_2 is formed from ^1S atomic states, and an MRCI is unnecessary to obtain a proper description of its formation. The QCISD[22,23] procedure was used to obtain the results reported here using a (14s,10p,2d,1f)/[7s,4p,2d,1f] basis set.[37] The predicted well depth, uncorrected for basis set superposition error, is 1.48×10^{-2} ev, a value greater than the experimental one of 1.22×10^{-2} ev.[38] The calculated minimum is found at a separation of 7.05 au compared to a recent theoretical and experimental value of 7.13 au.[38]

The molecular charge distributions depicted in Figure 11 show that the formation of the Ar_2 molecule is primarily the result of a simple merging, that is, addition of the two atomic distributions with little accompanying reorganization. It is a characteristic of such closed-shell interactions that the value of ρ_b, as well as being relatively small, Figure 12a, is given approximately by the sum of the densities of the free atoms evaluated at distances equal to their bonded radii in the molecule, a value labeled ρ_b^o.[39] For example at R_e, $\rho_b = 3.19 \times 10^{-3}$ and $\rho_b^o = 3.32 \times 10^{-3}$ au for Ar_2.

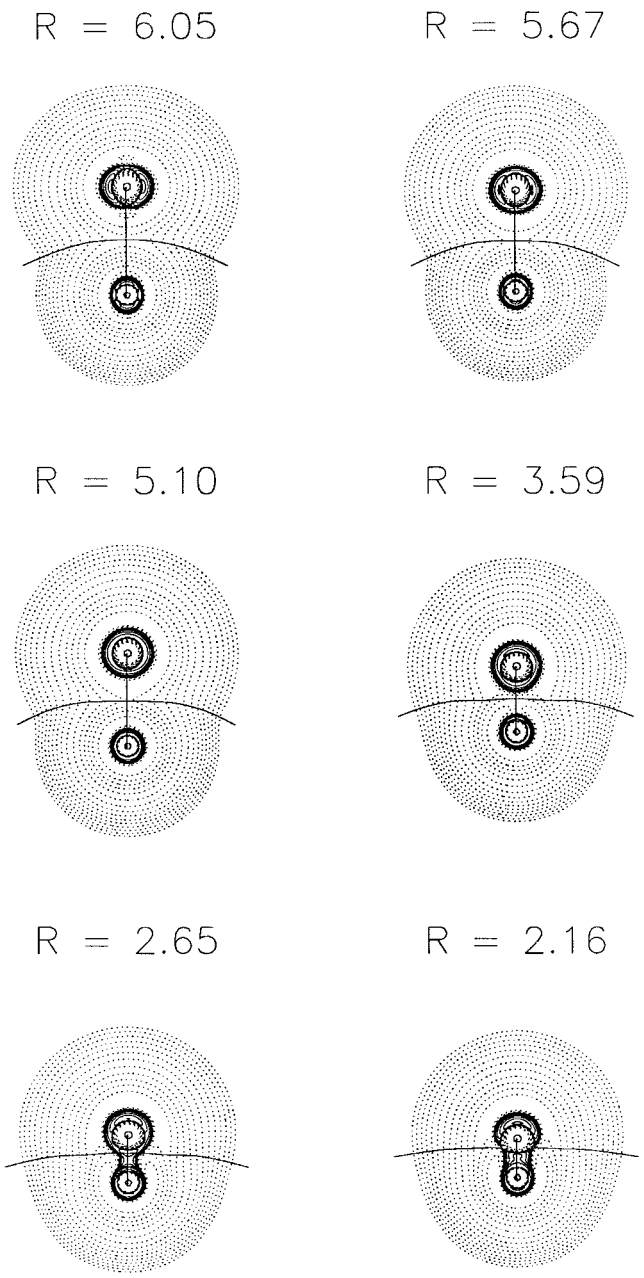

Figure 10. Laplacian of the electron density for CO as a function of *R*. Note the transformation of the torus of charge concentration on carbon (the upper atom) for large *R* into axial bonded and nonbonded charge concentrations at R_e.

The bond CP properties exhibit values reflecting the mechanics of a closed-shell interaction and are similar to those previously reported in a study of van der Waals molecules.[39] Since density is not accumulated in the region of the bond CP, the value of ρ_b being instead approximately equal to the sum of the atomic densities for the same degree of penetration, the sign of $\nabla^2\rho_b$ is determined by the positive axial curvature of the density for all separations, Figure 12a. By the local viriral theorem eq 8, the interaction is dominated by the kinetic energy contribution to the energy density. Thus the energy density H_b, like $\nabla^2\rho_b$, is positive at all separations, and the CP data at R_e exhibit the same characteristics as found for the interaction of the closed-shell ions in LiF, Table 1. For separations greater

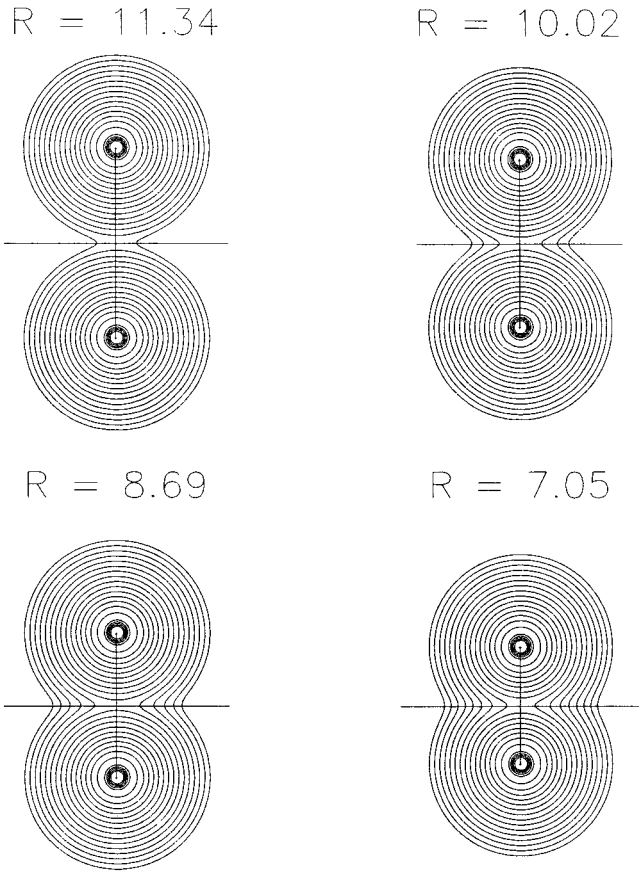

Figure 11. Evolution of the density distribution of Ar_2. Aside from the region of overlap, no distortions of the atomic forms of the density are discernible.

than 11 au, each atom is polarized toward the other, following which the atomic dipoles are reversed, Figure 12b. The atomic quadrupole polarizations exhibit paralleling behavior. At distances greater than 11 au, $Q_{zz}(Ar) < 0$ and density is accumulated along the axis of approach, but a further decrease in R causes a reversal of this polarization resulting in a removal of electron density from along the axis and placing it in a torus-like distribution about the axis within each atomic basin, Figure 12c. Such dipolar and quadrupolar polarizations remove density from the region of overlap and facilitate the approach of two closed-shell atoms or ions. Recall that $Q_{zz}(F) > 0$ for LiF at R_e.

Once there is effective overlap of the density distributions of the argon atoms as occurs for $R < 10$ au and as evident in the steep rise in ρ_b, the density behaves in such a manner as to facilitate the mutual penetration of the two atomic densities, behavior typical of closed-shell interactions that involve little or no charge transfer.[39] This includes hydrogen bond formation which exhibits the same characteristics; $\rho_b \sim \rho_b^o$ and the densities of both the base atom and hydrogen polarize away from one another and both undergo quadrupolar polarizations that remove density from along the axis of approach.[40] One finds that the strength of the hydrogen bond is directly proportional to the degree of interpenetration of the densities of the hydrogen and base atoms, that is, with the value of the density at the hydrogen bond CP. Thus, penetration with the accompanying polarizations that facilitate it is the mechanism employed to achieve binding in a closed-shell interaction. Unlike a shared interaction which accumulates density in the binding region well in excess of that obtained by the simple overlap of the atomic densities, the penetration mechanism is limited to generating a value of ρ_b that is approximately equal to ρ_b^o, the corresponding sum of the unperturbed atomic densities. Unless preceded by and resulting from a significant interatomic charge transfer, as occurs in an ionic interaction or one produced by the approach of two polar species as can occur in the formation of a hydrogen bond, such a reorganization of the density yields a weak interaction. Despite the lack of charge accumulation in the binding region relative to the value of ρ_b^o, a (3,−1) CP exists between the nuclei. Its presence, because of its associated topological properties, ensures that the nuclei are linked by a bond path, a line along which the electron density is a maximum with respect to any neighboring line. Coexisting with the bond path is a virial path, a line of maximally negative potential energy density.

The perturbations in the densities of the argon atoms, induced by their interpenetration required to attain an equilibrium geometry, are orders of magnitude smaller than those encountered in the shared, polar, and ionic interactions. The perturbations induced in the VSCC are correspondingly slight but yield a pattern of partial pair condensation similar to that found for the shared and polar interactions. Thus, axial bonded and nonbonded CCs are formed in the VSCC of each atom in the equilibrium charge distribution and they are linked by a torus of (2,0) CPs encircling the axis that is displaced 0.56 au toward the nonbonded side of each nucleus. The magnitudes of the bonded and nonbonded maxima in $\nabla^2\rho$ exceed those of the minima in the VSCC of an Ar atom by only 0.002 au. The values of $L(\mathbf{r})$ at these CPs and their radial distances are unchanged to three significant figures from those that characterize the sphere of maximum charge concentration in the VSCC of a free Ar atom, $L(\mathbf{r}) = 1.15$ au and $r = 1.09$ au. Thus the distortions of the VSCC and the extent of electron pairing are slight in the formation of van der Waals molecules, reflecting their small binding energies.

Energetics of Bonding and the Atomic Contributions. Slater regarded the virial and Hellmann−Feynman theorems as "two of the most powerful theorems applicable to molecules and solids",[41] and for an open system one must add to these the Ehrenfest force theorem. The virial theorem serves to relate the Ehrenfest and Hellmann−Feynman (H−F) forces to the behavior of the total energy and its kinetic and potential energy contributions, as a function of the separation between the two open atomic systems. For a molecule at a nonequilibrium separation, the virial contains a contribution from the external forces, the virial of the H−F forces acting on the nuclei, which, for a diatomic molecule, may be expressed as $R(dE/dR)$. The virial theorem itself may be expressed as in eq 9 in terms of the differences in the kinetic and total energies, $\Delta T(R)$ and $\Delta E(R)$, Δ denoting the difference between the molecular value at a given separation R and the value for the separated atoms for which $T(\infty) = -E(\infty)$

$$\Delta T(R) = -\Delta E(R) - R(dE/dR) = \Delta E(R) + RF(R) \quad (9)$$

Since the H−F force vanishes at R_e, the virial theorem requires that T increase in the formation of a bound state and that the increase equal the magnitude of the decrease in the total energy; that is, $\Delta T(R_e) = -\Delta E(R_e) = -{}^1/_2 V(R_e)$. However, for the molecules bound by shared interactions, H_2, N_2, and CO, the kinetic energy initially decreases in the region of attractive forces preceding R_e, Figure 13a, b, and c. The separation R_i is important in demarking the regions of increase and decrease in T. R_i is the point at which the attractive H−F force on a nucleus attains its maximum magnitude, corresponding to the inflection point on the $E(R)$ versus R curve and illustrated for H_2 in Figure 13d, the results for this system obeying both the virial and H−F

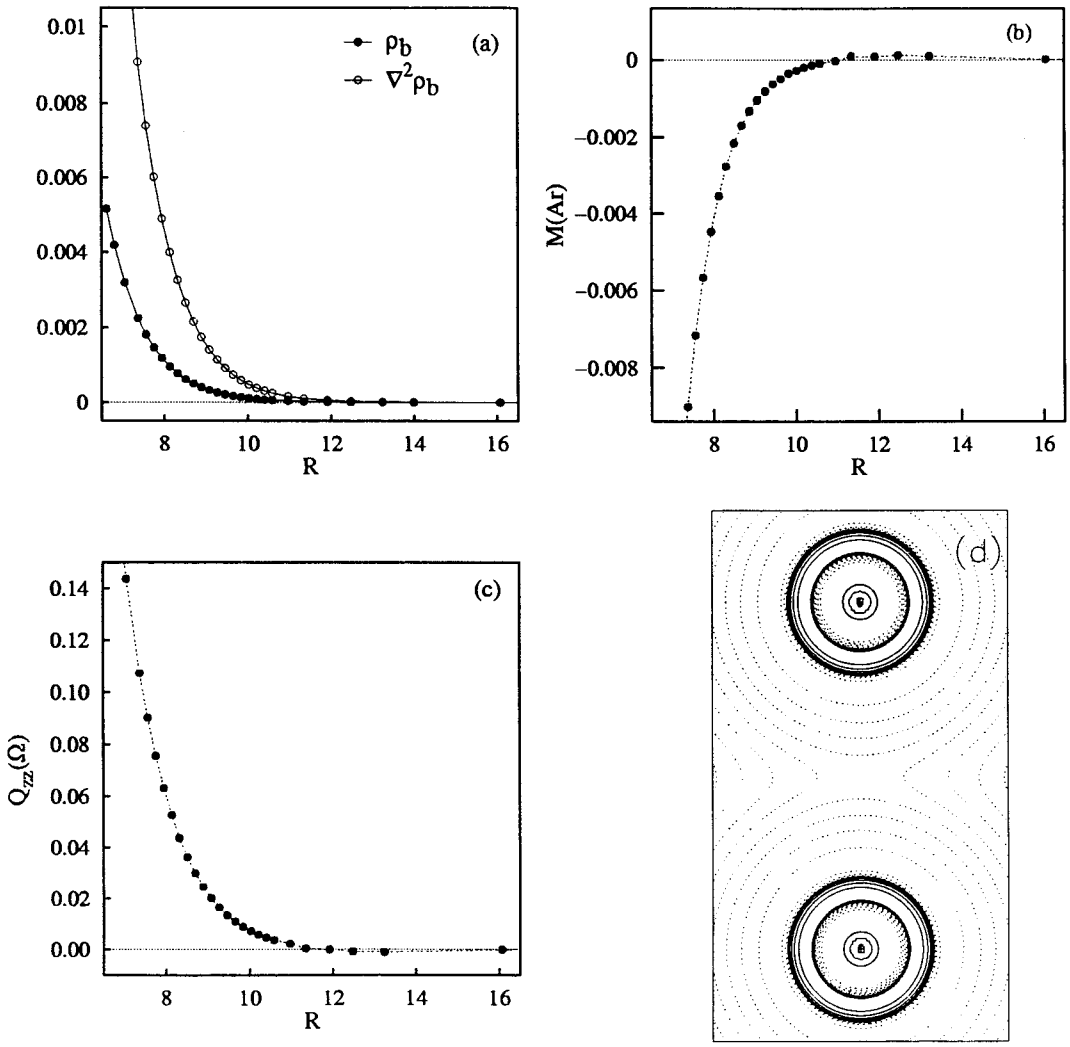

Figure 12. Atomic and bond properties of Ar_2 as a function of R: (a) density and its Laplacian at bond CP; (b) atomic polarization $\mathbf{M}(\Omega)$; (c) atomic quadrupole polarization with respect to the molecular axis, $Q_{zz}(\Omega)$; (d) equilibrium Laplacian distribution. No alterations of the VSCCs from their atomic forms are discernible in this diagram.

theorems. For H_2, the maximum force = 0.087 au (= 7.2 nN) occurs at $R \sim 2.1$ au. The virial theorem, through further differentiation with respect to R, can be used to obtain expressions for dT/dR and dV/dR.[1,42] These expressions show that for $R > R_i$ the signs of these two derivatives are not uniquely determined. However, for a system in which the term $R dF(R)/dR$ dominates the contribution from the force $F(R)$, the kinetic energy will initially decrease and the potential energy increase, as observed here for the three molecules with shared interactions. For $R = R_i$, the signs of the two derivatives are uniquely fixed with $dT/dR < 0$ and $dV/dR > 0$ and at this point and for a further decrease in R, T must increase and V must decrease to eventually satisfy the requirements of the virial theorem that $\Delta T(R_e) = -\Delta E(R_e)$ and $V(R_e) = 2\Delta E(R_e)$ for a bound state.

The initial decrease in T and increase in V observed for the shared interactions can be quantitatively accounted for. The region with $R \gg R_i$, characterized by attractive H−F forces and a decreasing electronic kinetic energy, is where dispersion forces are dominant. For the approach of two atoms in S states, the sole contribution to these forces comes from the long-range Coulomb correlation between the electrons on the two atoms. As first emphasized by Feynman,[43] dispersion forces, with their R^{-7} dependence for the approach of two neutral spherical atoms, result from a polarization of the density on each of the approaching atoms toward the other, leading to an increasing accumulation of density between the approaching nuclei and to the formation of a bond path.[4] The effect of the electron correlation on the distribution of density in real space has been previously illustrated in terms of a density difference map for the approach of two hydrogen atoms separated by 8 au.[1,44] The map demonstrates that for $R \gg R_i$ density is removed from the region of each nucleus, where the gradients of the wave function are large and leads to large local contributions to T and where the local potential energy is maximally stabilizing. It is accumulated in the form of a diffuse distribution removed from the immediate region of each nucleus and placed in the region between them, thereby accounting for the decrease in T and the increase in V accompanying the approach of the atoms. Thus the initially attractive forces acting on two approaching nuclei are boot-strap forces: each nucleus is pulled by its own inwardly polarized electron density distribution.

This long-range charge reorganization found for the H atoms has the effect of decreasing $|V_{ne}^{o}(H)|$, the attractive interaction of a proton with the electron density in its associated basin, the single largest contribution to the potential energy of an atom. This quantity parallels the behavior of the total potential energy for H_2, as shown in Figure 13a, which shows the contribution of $\Delta V_{ne}^{o}(H)$ as a function of R. The same behavior is found for the N atoms in forming N_2 , Figure 13b, where $\Delta V_{ne}^{o}(N)$ is shown divided by the nuclear charge Z to obtain values

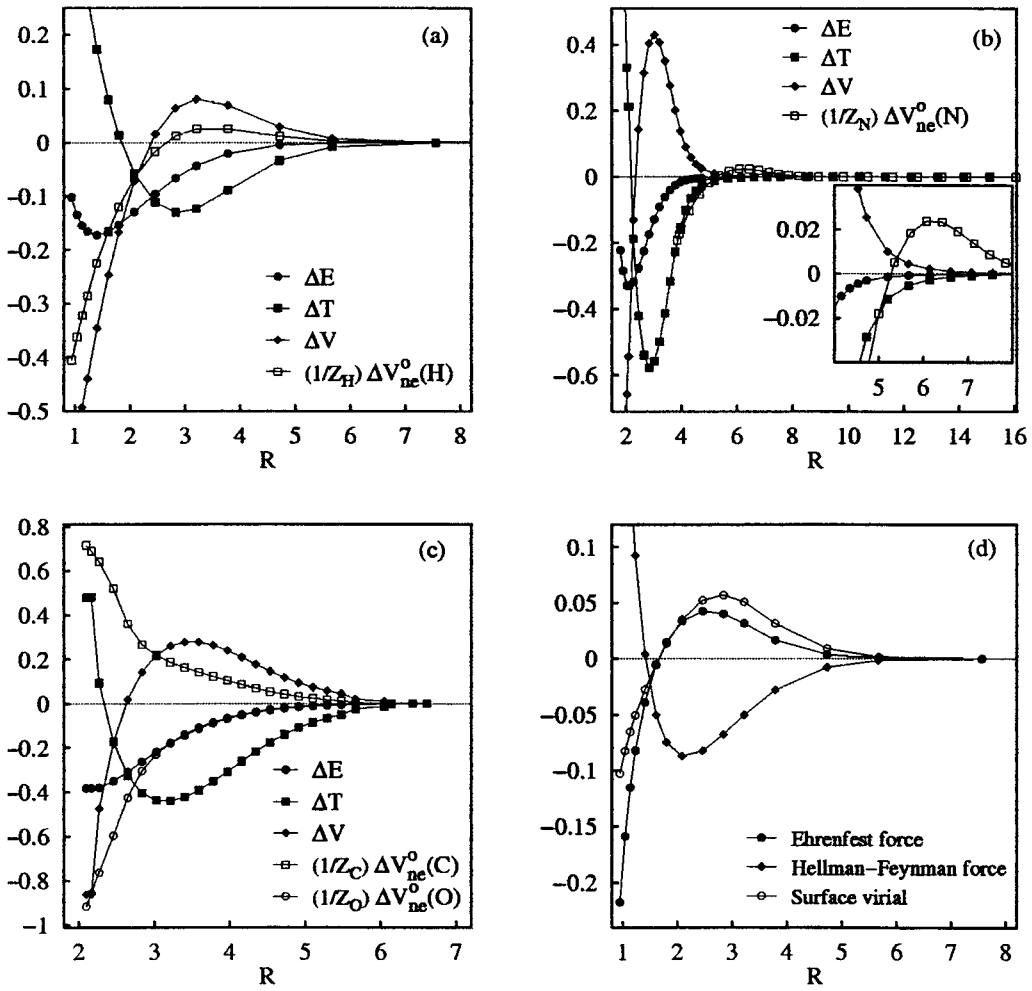

Figure 13. Changes in the total (ΔE), kinetic (ΔT), and potential (ΔV) energies relative to the separated atoms as a function of R for (a) H_2, (b) N_2, (c) CO. Also displayed is the change in the basin contribution to the electron−nuclear potential energy per nuclear charge, $(1/Z)V_{ne}^{o}(\Omega)$. The variation in the Ehrenfest force and the surface virial, eq 6, for an H atom in H_2 and the Hellmann−Feynman force on its nucleus is shown in (d). The surface virial in this case equals $(\mathbf{R}/2)\cdot\oint d\mathbf{S}\cdot\sigma$. The Hellmann−Feynman force attains its maximum attractive value for the separation R_i. The Ehrenfest force becomes negative and the surface virial stabilizes at a separation lying between R_i and R_e.

commensurate with the changes in the total energy contributions. The quantity ΔV_{ne}^{o}(C) for CO in Figure 13c exhibits a monotonic increase as R decreases, a result of the continuing loss of electronic charge to oxygen. ΔV_{ne}^{o}(O) does exhibit a small increase for R ∼, one that is quickly overwhelmed by the charge transfer.

For the region $R_i > R > R_e$, the overlap of the separate atomic wave functions becomes significant, leading to an increasing transfer and accumulation of electron density between the nuclei. It is in this range of R where the derivatives of T and V are such that T must increase and V must decrease to eventually satisfy the requirements of the virial theorem. The change in the nature of the interaction for H_2 and N_2 for passage into this range of internuclear separations is quantitatively monitored by the changes in ρ_b and $\nabla^2\rho_b$, Figure 6a. For the dispersion interactions preceding R_i, the value of ρ_b, the maximum value attained by ρ in the interatomic surface, is relatively small and $\nabla^2\rho_b > 0$, its value being dominated by the positive curvature of ρ along the bond path. The change in sign of $\nabla^2\rho_b$ and the rapid increase in ρ_b to values characteristic of a shared interaction that occurs at ∼ 3 au is a result of the contraction of the density toward the bond path that accompanies the increasing accumulation of density in the internuclear region. This is precisely the internuclear separation at which ΔT begins its steep increase and V an equally steep decrease in attaining the values characteristic of equilibrium, all three molecules exhibiting the same behavior.

Dispersion forces are responsible for the binding in Ar_2, and the behavior of this system for $R > 11$ au is the same as that found for large separations in H_2, with an initial decrease in T and increase in V, Figure 14a. There is also a small initial rise in the value of ΔV_{ne}^{o}(Ar) accompanied by atomic dipolar and quadrupolar polarizations that accumulate density in the binding region, the same mechanism underlying the attractive interaction found for H_2 at large separations. However, as noted above, these polarizations are reversed for $R < 10$ au, where the overlap of the atomic densities becomes significant, forcing the onset of the penetration mechanism for the approach of two closed-shell systems.

In the formation of LiF, there is a rapid initial increase in T and decrease in V accompanying the abrupt transfer of electron density from Li to F, both quantities exhibiting extrema in the neighborhood of 10 au where the charge transfer is essentially complete, Figure 14b. The subsequent decrease in T and increase in V can again be traced to an increase in the nuclear−electron attractive interaction within the atomic basins, particularly for F, with ΔV attaining its maximum value at ∼6 au. The corresponding quantity for Li exhibits an increase even for very large R, a result of its loss in density to the F atom. However, ΔV_{ne}^{o}(Li) does attain a maximum value at $R = 7$ au and

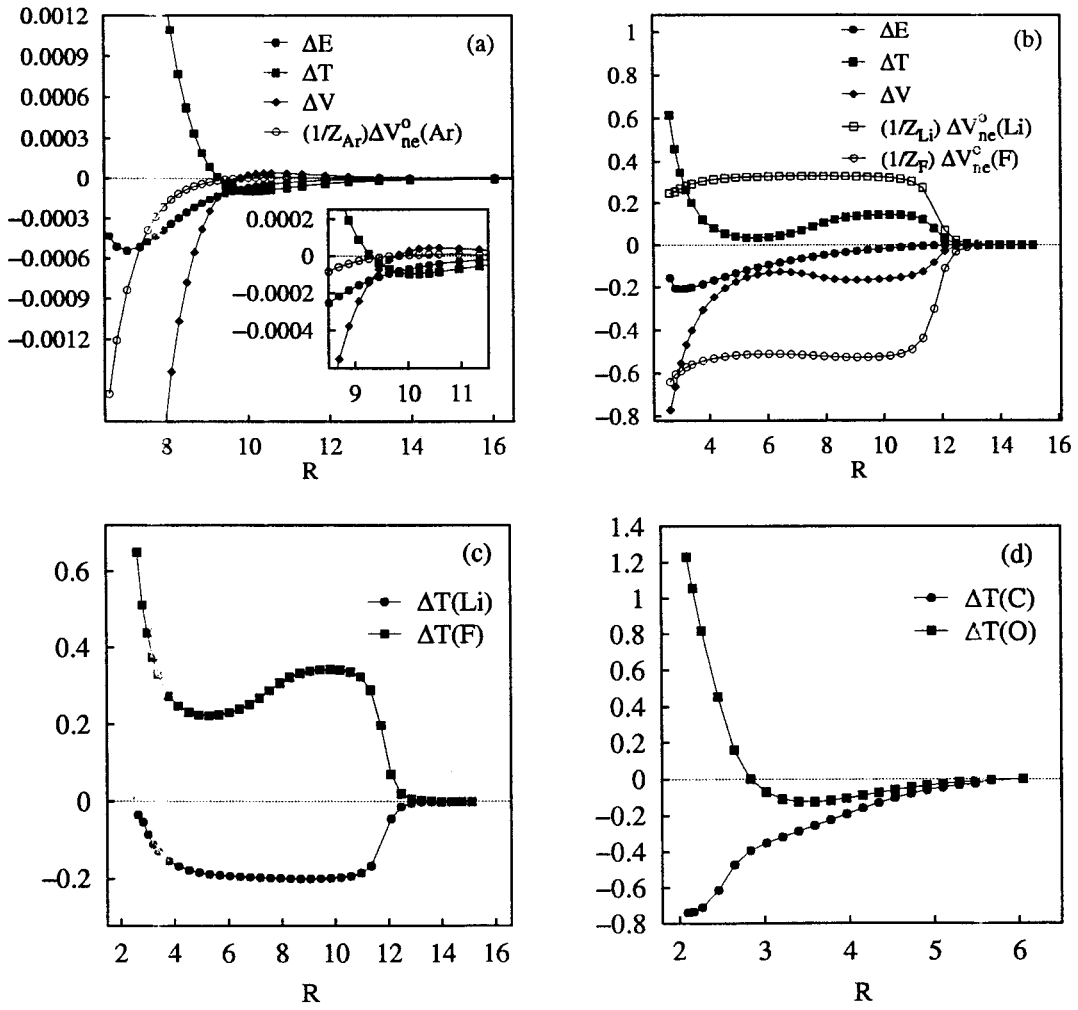

Figure 14. Changes in the total, kinetic, and potential energies and in $(1/Z)V_{ne}^{o}(\Omega)$ relative to the separated atoms as a function of R for Ar_2 in (a) and LiF in (b). Atomic contributions to the changes in the electronic kinetic energies for LiF in (c) and CO in (d).

continues to decrease for further decrease in R. Thus LiF, particularly the F atom, following the abrupt interatomic charge transfer, exhibits the characteristic expansion of its density that results in a decrease in T and an increase in V at large internuclear separations.

Figures 14c and d show the contribution of each atom to the changes in the kinetic energy for the heteronuclear systems. At the equilibrium separation, $\Delta T(\mathrm{A}) = -\Delta E(\mathrm{A})$, the change in the energy of atom A in forming the molecule AB. In each case, the atom that loses electron density, A = C or Li, undergoes an understandable decrease in its average kinetic energy and is destabilized in the molecule, relative to the separated atom. It is the increase in $\Delta T(\mathrm{B})$, the kinetic energy of the electronegative atoms B = O or F, that exceeds the magnitude of the decrease in $\Delta T(\mathrm{A})$ and accounts for the stability of the molecule. Note that $\Delta T(\mathrm{O})$ clearly exhibits the initial decrease in T that is characteristic of the shared interactions, a decrease that is almost masked in the value of ΔT because of the contribution from the carbon atom. Similarly, $\Delta T(\mathrm{F})$ mimics the behavior of ΔT by showing a decrease in value following the transfer of charge that is essentially complete by 10 au.

The Ehrenfest Force. The atomic Ehrenfest force**,** the quantity $\mathbf{F}(\Omega)$ in eq 4, exhibits an extremum for decreasing R, as does the Hellmann−Feynman force. In H_2, $\mathbf{F}(\mathrm{H})$ attains a maximum value of 0.043 au (= 3.5 nN) for $R \sim 2.5$ au, a separation that is in slight excess of R_i, Figure 13d. A positive Ehrenfest force in the present instance means that each atom experiences a force directed away from its neighbor − away from the interatomic surface. At a value of R slightly greater than R_e, the Ehrenfest force changes sign and each atom experiences a force drawing it toward its neighbor − toward the interatomic surface. The Ehrenfest force vanishes and subsequently changes sign when the electrostatic force of attraction exerted on the electron density in the atomic basin by the nuclei is balanced by the repulsive force exerted by the electrons, the latter force including the quantum effects of exchange and correlation, in addition to the Coulomb interaction. The force required to rupture a single covalent bond was recently measured in an atomic force microscope (AFM) by stretching the bond between two atoms, one being linked to the tip of the microscope, the other to a surface.[46] If an H−H bond is so stretched when one atom, say H_t, is linked to the tip of an AFM and the other, H_s, to the surface of some material, the tip together with H_t form an open system, H_s, and the surface to which it is bound, referred to collectively as the sample, forming another. The two open systems are separated by the H−H interatomic surface, and the force exerted on the tip of the AFM is a result of the pressure exerted by the sample on each element of the interatomic surface, eq 4.[8] The measured force would be classed as attractive in the region where $\mathbf{F}(\mathrm{H_t}) > 0$, since it would be opposing the force exerted by the sample that draws H_t and the tip toward the surface. Recall that $\mathbf{F}(\mathrm{H_t}) = -\oint \mathrm{d}\mathbf{S}\cdot\sigma = -\mathbf{F}(\mathrm{H_s})$ and the force measured in the AFM is equal to $-\mathbf{F}(\mathrm{H_s})$. The bond would

TABLE 2: Ehrenfest Forces (in atomic units) for Equilibrium Geometries[a]

AB	$\mathbf{F}(\Omega)$	$\mathbf{F}_{e\beta}(\Omega)$	$\mathbf{F}_{e\alpha}(\Omega)$	$\mathbf{F}_{ee}(\Omega,\Omega+\Omega,\Omega')$
H(H)	−0.0391	+0.1681	−0.3365	+0.1293
N(N)	−0.0653	+1.5212	−9.8539	+8.2669
Ar(Ar)	−0.0028	+0.0046	−6.5141	+6.5067
C(O)	−0.9804	+4.3035	−12.342	+7.0580
(C)O	+0.9804	+6.2009	+1.8358	−7.0563
Li(F)	−0.0939	+0.6697	−3.1883	+2.4247
(Li)F	+0.0939	+2.0140	+0.0748	−1.9949

[a] Values refer to bracketed atom. Atom B is on the positive z axis and a positive force is directed away from atom A. A positive force for atom A is directed at atom B.

rupture when the force applied to the lever arm of the AFM equalled the maximum value displayed in the curve for $\mathbf{F}(H)$ shown in Figure 13d. For shorter separations, where $\mathbf{F}(H_t) < 0$, the measured Ehrenfest force would be classed as repulsive, as it would be opposed by a force pushing against the interatomic surface that H_t shares with H_s. The Ehrenfest force for H_2 is of the same order of magnitude as the Hellmann−Feynman forces on the nuclei, Figure 13d. Results similar in all respects, attractive for large R and becoming repulsive for a value of R somewhat greater than R_e, are found for the formation of N_2 and CO. Thus the Ehrenfest force for an atom in N_2, $\mathbf{F}(N)$, exhibits a maximum value of 12 nN at $R = 2.5$ au ($R_e = 2.07$ au), while the magnitude of the Hellmann−Feynman force on an N nucleus attains a maximum value of 17 nN at a still greater separation of 2.8 au.

In a diatomic molecule AB, the Ehrenfest force is given by

$$\mathbf{F}(A) = \mathbf{F}_{e\beta}(A) + \mathbf{F}_{e\alpha}(A) + \mathbf{F}_{ee}(A,A) + \mathbf{F}_{ee}(A,B) \quad (10)$$

where $\mathbf{F}_{e\alpha}(A)$ and $\mathbf{F}_{e\beta}(A)$ are the forces exerted on the electron density in atom A by nucleus α of atom A and nucleus β of atom B and where $\mathbf{F}_{ee}(A,A)$ and $\mathbf{F}_{ee}(A,B)$ are the forces exerted on the electron density in atom A by the density in A and by that in B. The force $\mathbf{F}_{e\beta}(A)$ draws the density of atom A toward the interatomic surface, toward B, while $\mathbf{F}_{e\alpha}(A)$ may be may be directed at B or away from it depending on the direction of polarization of the density on A. Similarly, $\mathbf{F}_{ee}(A,B)$ is directed away from B while $\mathbf{F}_{ee}(A,A)$ may be directed either toward or away from atom B. The Ehrenfest force acting on the atoms at R_e in the second-row homonuclear diatomics and in the diatomic hydrides is found to be such that each atom is pulled toward its neighbor, the same result being found for the molecules studied here, Table 2, giving the nuclear and electronic contributions to $\mathbf{F}(A)$ at R_e. Atom B is on the positive z axis and thus a negative force draws it toward A. In each case, the contribution to the atomic Ehrenfest force with the greatest magnitude is the force exerted by the nucleus of the neighboring atom which draws the atoms together. Because the density of each atom in CO and LiF is polarized in a direction counter to the charge transfer, all four nuclei exert forces on their own atomic densities in the positive direction, toward the interatomic surface for C and Li and away from the surface for O and F. All of the molecules exhibit a rapid increase in the magnitude of the atomic Ehrenfest force dawing the atom toward its neighbor for separations less than R_e as found for H_2, Figure 13d. The rate of increase is greater for the polar CO molecule, and the atomic Ehrenfest force acting in this molecule at R_e is larger by a factor of 10 than for the ionic interaction found in LiF, which in turn is greater than that found in the shared interactions N_2 and H_2. A correspondingly large Ehrenfest force is found acting in the interatomic surface of CN in an amide linkage,[45] where the surface exhibits the same characteristic shape determined by the core of the carbon atom, as found for CO, Figure 8. Such a large Ehrenfest force should be apparent in atomic force microscope measurements that are now used to determine the force required to separate a pair of atoms by the breaking of an individual bond.[46]

Acknowledgment. One of us (J.H.-T.) acknowledges financial support from CONACYT-México which made this work possible. We wish to thank Dr. C. Gatti and Dr. V. Luaña for helpful discussions.

References and Notes

(1) Bader, R. F. W. *Atoms in Molecules − A Quantum Theory*; Oxford University Press: Oxford, U.K., 1990.
(2) Bader, R. F. W. *Phys. Rev. B* **1994**, *49*, 13348.
(3) Bader, R. F. W.; Popelier, P. L. A.; Keith, T. A. *Angew. Chem., Int. Ed. Engl.* **1994**, *33*, 620.
(4) Bader, R. F. W. *J. Phys. Chem. A* **1998**, *102*, 7314.
(5) Schwinger, J. *Phys. Rev.* **1951**, *82*, 914.
(6) Schrödinger, E. *Ann. Phys.* **1926**, *79*, 361.
(7) Bader, R. F. W.; Popelier, P. A. L. *Int. J. Quantum Chem.* **1993**, *45*, 189.
(8) Bader, R. F. W. *Phys. Rev. B*, accepted for publication.
(9) Keith, T. A.; Bader, R. F. W.; Aray, Y. *Int. J. Quantum Chem.* **1996**, *57*, 183.
(10) Cremer, D.; Kraka, E. *Angew. Chem.* **1984**, *23*, 627.
(11) Magee, J. L. *J. Chem. Phys.* **1940**, *8*, 687.
(12) Werner, H.-J.; Meyer, W. *J. Chem. Phys.* **1981**, *74*, 5802.
(13) Herschbach, D. R. *Adv. Chem. Phys.* **1966**, *10*, 319.
(14) Bauschlicher, C. W.; Langhoff, S. R. *J. Chem. Phys.* **1988**, *89*, 4246.
(15) Schmidt, M. W.; Baldridge, K. K.; Boate, J. A.; Elbert, S. T.; Gordon, M. S.; Jensen, J. H.; Koseki, S.; Matsunaga, N.; Nguyen, K. A.; Su, S. S.; Windus, T. L.; M. Dupuis, M.; Montgomery, J. A. GAMESS, *J. Comput. Chem.* **1993**, *14*, 1347.
(16) Sadlej, A. J. *Collect. Czech. Chem. Commun.* **1988**, *53*, 1995.
(17) Sadlej, A. J.; Urban, M. *J. Mol Struct. (THEOCHEM)* **1991**, *234*, 147.
(18) Bader, R. F. W.; Henneker, W. H. *J. Am. Chem. Soc.* **1965**, *87*, 3063. Bader, R. F. W.; Henneker, W. H.; Cade, P. E. *J. Chem. Phys.* **1967**, *46*, 3341.
(19) Bader, R. F. W.; MacDougall, P. J.; Lau, C. D. H. *J. Am. Chem. Soc.* **1984**, *106*, 1594.
(20) Bader, R. F. W.; Heard, G. L. *J. Chem. Phys.* **1999**, *11*, *8789*.
(21) Kolos, W.; Szalewicz, K.; Monkhorst, H. J. *J. Chem. Phys.* **1986**, *84*, 3278.
(22) Pople, J. A.; Head-Gordon, M. *J. Chem. Phys.* **1987**, *87*, 5968.
(23) Frisch, M. J.; Trucks, G. W.; Schlegel, H. B.; Gill, P. M. W.; Johnson, B. G.; Robb, M. A.; Cheeseman, J. R.; Keith, T.; Petersson, G. A.; Montgomery, J. A.; Raghavachari, K.; Al-Laham, M. A.; Zakrzewski, V. G.; Ortiz, J. V.; Foresman, J. B.; Cioslowski, J.; Stefanov, B. B.; Nanayakkara, A.; Challacombe, M.; Peng, C. Y.; Ayala, P. Y.; Chen, W.; Wong, M. W.; Andres, J. L.; Replogle, E. S.; Gomperts, R.; Martin, R. L.; Fox, D. J.; Binkley, J. S.; Defrees, D. J.; Baker, J.; Stewart, J. P.; Head-Gordon, M.; Gonzalez, C.; Pople, J. A. *Gaussian 94*, Revision E.2, Gaussian, Inc.: Pittsburgh, PA, 1995.
(24) LeRoy, R. J.; Barwell, M. G. *Can. J. Phys.* **1975**, *53*, 1983.
(25) Werner, H.-J.; Knowles, P. J. *J. Chem. Phys.* **1991**, *94*, 1264.
(26) Almlöf, J.; Deleeuw, B. J.; Taylor, P. R.; Bauschlicher, C. W.; Siegbahn, P. *Int. J. Quantum Chem. Symp.* **1989**, *23*, 345.
(27) Langhoff, S. R.; Bauschlicher, C. W.; Taylor, *Chem. Phys. Lett.* **1991**, *180*, 88.
(28) Halkier, A.; Helgaker, T.; Jørgensen, P.; Klopper, W.; Koch, H.; Olsen, J.; Wilson, A. K. *Chem. Phys. Lett.* **1998**, *286*, 243.
(29) Ganturco, F. A.; Schneider, F. *Mol. Phys.* **1996**, *89*, 753.
(30) Huber, K. P.; Herzberg, G. *Molecular Spectra and Molecular Structure, IV. Constants of Diatomic Molecules*; Van Nostrand: New York, 1979.
(31) Krokidis, X.; Noury, S.; Silvi, B. *J. Phys. C.* **1997**, *101*, 7277. Noury, S.; Colonna, F.; Savin, A.; Silvi, B. *J. Mol. Struct.* **1998**, *450*, 59.
(32) Becke, A. D.; Edgecombe, K. E. *J. Chem. Phys.* **1990**, *92*, 5397.
(33) Ponec, R. *Croatica Chem. Acta* **1997**, *70*, 745. Ponec, R.; Carbo-Dorca, R. *Int. J. Quantum Chem.* **1999**, *72*, 85.
(34) Peterson, K. A.; Dunning, T. H. *J. Mol. Struct. (THEOCHEM)* **1997**, *400*, 93.
(35) Dunning, T. H. *J. Chem. Phys.* **1989**, *90*, 1007.
(36) Muenter, J. S. *J. Mol. Spectrosc.* **1975**, *55*, 490.
(37) Chalasinski, G.; Funk, D. J.; Simons, J.; Breckenridge, W. H. *J. Chem. Phys.* **1987**, *87*, 3569.

(38) Woon, D. E. *Chem. Phys. Lett.* **1993**, *204*, 29.
(39) Bone, R. G. A.; Bader, R. F. W. *J. Phys. Chem.* **1996**, *100*, 10892.
(40) Carroll, M. T.; Bader, R. F. W. *Mol. Phys.* **1988**, *65*, 695.
(41) Slater, J. C. *J. Chem. Phys.* **1972**, *57*, 2389.
(42) Bader, R. F. W. In *The Force Concept in Chemistry*; Van Nostrand Reinhold Co.: New York, 1981; p 39.
(43) Feynman, R. P. *Phys. Rev.* **1939**, *56*, 340.
(44) Bader, R. F. W. *Introduction to the Electronic Structure of Atoms and Molecules*; Clarke Irwin and Co. Ltd.: Toronto, 1970.
(45) Bader, R. F. W.; Martin, F. J. *Can. J. Chem.* **1998**, *76*, 284.
(46) Grandbois, M.; Beyer, M.; Rief, M.; Clausen-Schaumann, H.; Gaub, H. E. *Science* **1999**, *283*, 1727.